Research article

Biological evaluation of novel side chain containing CQTrICh-analogs as antimalarials and their development as *Pf*CDPK1 kinase inhibitors

Iram Irfan [a], Amad Uddin [a,b,#], Ravi Jain [b], Aashima Gupta [b], Sonal Gupta [b,1], John V. Napoleon [c], Afzal Hussain [d], Mohamed F. Alajmi [d], Mukesh C. Joshi [e], Phool Hasan [a], Purnendu Kumar [b], Mohammad Abid [a,**], Shailja Singh [b,*]

[a] *Medicinal Chemistry Laboratory, Department of Biosciences, Jamia Millia Islamia, New Delhi, 110025, India*
[b] *Special Centre for Molecular Medicine, Jawaharlal Nehru University, New Delhi 110067, India*
[c] *Chemistry, Purdue University System, West Lafayette, IN, USA*
[d] *Department of Pharmacognosy, College of Pharmacy, King Saud University, Riyadh, Saudi Arabia*
[e] *Department of Chemistry, Kirori Mal College, University of Delhi, Delhi 110007, India*

ABSTRACT

The rapid emergence of resistance to existing frontline antimalarial drugs emphasizes a need for the development of target-oriented molecules with novel modes of action. Given the importance of a plant-like Calcium-Dependent Protein Kinase 1 (*Pf*CDPK1) as a stand-alone multistage signalling regulator of *P. falciparum*, we designed and synthesized 7-chloroquinoline-indole-chalcones tethered with a triazole (CQTrICh-analogs **7 (a–s)** and **9**) directed towards *Pf*CDPK1. This was accomplished by reacting substituted 1-phenyl-3-(1-(prop-2-yn-1-yl)-1H-indol-3-yl) prop-2-en-1-one and 1-(prop-2-yn-1-yl)-1H-indole-3-carbaldehyde with 4-azido-7-chloroquinoline, respectively via a 'click' reaction. The selected CQTrICh-analogs: **7l** and **7r** inhibited the growth of chloroquine-sensitive 3D7 strain and -resistant RKL-9 isolate of *Plasmodium falciparum*, with IC$_{50}$ values of **2.4 μM** & **1.8 μM** (**7l**), and **3.5 μM** & **2.7 μM** (**7r**), respectively, and showed no apparent hemolytic activity and cytotoxicity in mammalian cells. Intra-erythrocytic progression studies revealed that the active hybrids: **7l** and **7r** are effective against the mature stages of the parasite. **7l** and **7r** were found to stably interact with the catalytically active ATP-binding pocket of *Pf*CDPK1 via energetically favourable H-bonds. The interaction was confirmed *in vitro* by microscale thermophoresis and kinase assays, which demonstrated that the active hybrids interact with *Pf*CDPK1 and inhibit its kinase activity which is presumably responsible for the parasite growth inhibition. Interestingly, **7l** and **7r** showed no inhibitory effect on the human kinases, indicating their selectivity for the parasite kinase. We report the antiplasmodial potential

* Corresponding author.
** Corresponding author.
E-mail addresses: iramirfanchem@gmail.com (I. Irfan), amaduddin4790@gmail.com (A. Uddin), ravijain28011989@gmail.com (R. Jain), aashimagupta1298@gmail.com (A. Gupta), sonal01g@gmail.com (S. Gupta), johnvictor.iitm@gmail.com (J.V. Napoleon), afzal.hussain.amu@gmail.com (A. Hussain), alajmister@gmail.com (M.F. Alajmi), mukeshjoshi21@gmail.com, mukeshjoshi21@kmc.du.ac.in (M.C. Joshi), phool.hassan@gmail.com (P. Hasan), purnendukumar450@gmail.com (P. Kumar), mabid@jmi.ac.in (M. Abid), shailjasingh@mail.jnu.ac.in (S. Singh).
[#] Current address: Department of Pharmacology and Chemical Biology, Emory University, School of Medicine, Atlanta, GA, USA.
[1] Current address: ICMR- National Institute of Malaria Research (Delhi campus), Sector 8, Dwarka, New Delhi-110077, India.

of novel kinase-targeting bio-conjugates, a step towards developing pan-kinase inhibitors which is a prerequisite for multistage anti-malarial protection.

1. Introduction

Side chains containing quinoline analogs constitute an important class of antimalarial drugs [1]. Consequently, there is an urgent need for novel approaches combating anti-malarial resistance and low-cost new drugs with favourable safety profiles [2–5]. According to the WHO report (2021), there were an estimated 241 million malaria cases and 627,000 deaths worldwide in 2020 [6]. It is, therefore, crucial to develop effective anti-malarial medications particularly those with novel mechanisms of action and favourable toxicity profiles, to combat malaria in the endemic regions. The side chain containing aminoquinolines (*viz.* chloroquine) is well known for inhibiting the conversion of Fe(III) heam to β-hematin and hemozoin [7,8]. Numerous studies have indicated that side-chain alteration and modifications may enhance antimalarial activity against various *P. falciparum* strains [9–14].

Researchers are actively exploring mechanistic approaches to understand how diverse antimalarials impede the *Plasmodium* parasite at different stages of its life cycle, yet the pursuit continues to pose significant challenges. Several groups are working to design and develop small molecular probes using various synthetic and biological approaches to understand their mode of action in the parasite's life cycle. Substituted heterocyclic compounds, synthesized by the fusion of two or more active pharmacophores, have been critical towards the development of anti-microbial medications. Towards this, chalcones and quinoline-based heterocycles are well-known in medicinal chemistry for their anti-bacterial, anti-inflammatory, analgesic, anti-malarial, anti-cancer, anti-viral, anti-leishmanial, and anti-tubercular effects. Such compounds have also been a primary source of inspiration for the development of new potent anti-malarial inhibitors. In this direction, E. M. Guantai synthesized and evaluated a targeted series of chalcone and dienone hybrid compounds, containing aminoquinoline and nucleoside templates, for an *in vitro* anti-malarial activity [15]. In this study, Cu (I)-catalyzed cyclo-addition of azides and terminal alkynes was applied as the hybridization strategy, and the most active chalcone-chloroquinoline based hybrid compound exhibited an IC$_{50}$ of 0.04 μM against D10 strain of *P. falciparum*. In the subsequent year, F. Shah et al. identified an indole-triazole based hybrid molecule against FP-2, by using structure-based virtual screening of a *focused* cysteine protease inhibitor library, followed by enrichment studies [16]. Biological evaluation revealed its IC$_{50}$ value of 4.59 μM against chloroquine-resistant (W2) strain of *P. falciparum*. Concomitantly, K. V. Sashidhara et al. synthesized chalcone-quinoline hybrids that showed comparable anti-malarial activity, at par with chloroquine, against the chloroquine sensitive 3D7 strain of
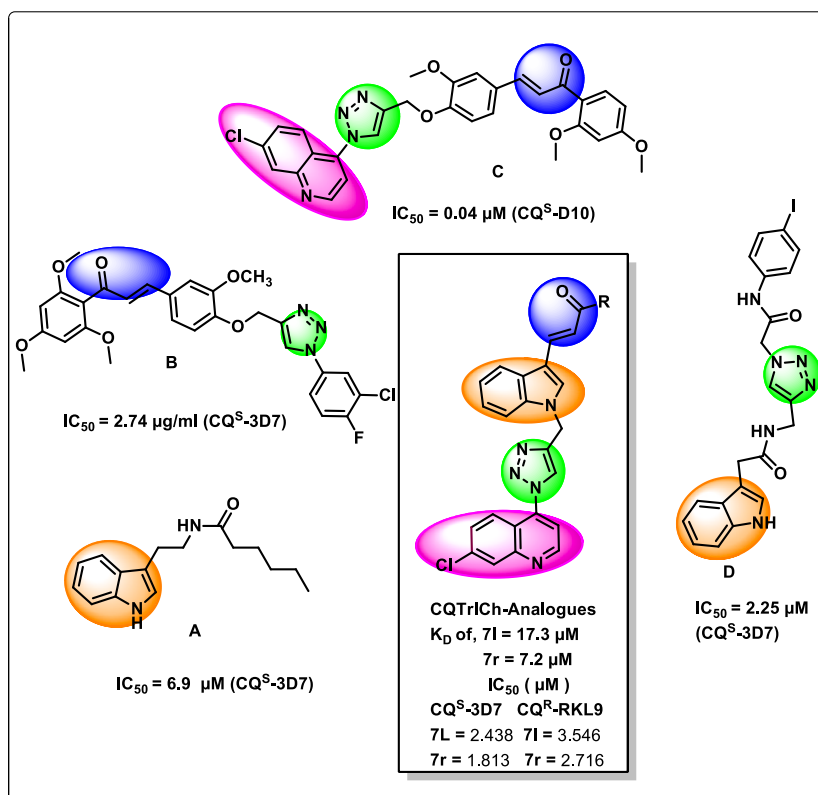

Fig. 1. Rationale for the design and development of CQTrICh-analogs.

P. falciparum, with an IC$_{50}$ value of 3.63 nM [17]. Moreover, the potent compounds showed significant *in vivo* efficacy in Swiss mice against chloroquine resistant N-67 strain of *P. yoelii*. Later, R. Kant et al. used copper catalyzed click chemistry to synthesize a series of 1,2,3-triazole linked chalcone and flavone hybrid molecules, which were further characterized as anti-bacterial, anti-fungal, and anti-plasmodial agents [18]. The potent hybrid compound was found to be active against *P. falciparum* strain 3D7, with an IC$_{50}$ of 2.74 μg/mL. In the following year, N. Devander et al. developed and synthesized an indoleamide derivative bearing a triazole pharmacophore, that demonstrated remarkable anti-plasmodial action *in vitro*, with an IC$_{50}$ of 2.25 μM against the chloroquine-sensitive *P. falciparum* 3D7 strain [19]. Later, a series of 1,2,3-triazole-naphthoquinone conjugates were synthesized by Royo et al., via Copper-catalyzed Azide-Alkyne Cycloadditions (CuAAC) and evaluated for their *in vitro* anti-malarial activity against chloroquine-sensitive strains of *P. falciparum* [20]. The two most active anti-malarial compounds showed IC$_{50}$ of 0.8 and 1.2 μM. Triazole based anti-malarial compounds have been developed. In the same year, Ishan Wadi et al. synthesized novel 4-amino-7-chloroquinoline-based 1,2,3-triazole hybrids by Cu^{I}-catalyzed Huisgen 1,3-dipolar cycloaddition reactions of 2-azido-N-(7-chloroquinolin-4-ylaminoalkyl)acetamides with various terminal alkynes, and the lead compounds were appreciably more active than chloroquine against the RKL-9 strain, along with gametocytocidal activity [21].

Calcium-Dependent Protein Kinase 1 (*Pf*CDPK1) is a biological target that may act as a vital point for the incoming probes. In the genus *Plasmodium*, CDPKs represent a class of serine/threonine protein kinases activated by Ca^{2+}-ions. This multigene family comprises seven members, and each gene is predominantly expressed in a distinct phase of the parasite life cycle. Since they are not found in mammals, CDPKs could serve as safer pharmacological targets. Previous reports highlight the relevance of *Pf*CDPK1 in *all* asexual intra-erythrocytic stages of the parasite, regulating the actin-myosin motor during gliding motility of *Plasmodium* merozoites and erythrocyte invasion, as well as the cAMP-mediated signalling cascade module [22]. Recognizing *Pf*CDPK1's critical function in the parasite life cycle, we investigated it as a potential target for the development of new anti-malarial drugs capable of inhibiting parasite growth by targeting *multiple* asexual stages in malarial infection.

Earlier attempts have been made to identify specific inhibitors against *Pf*CDPK1, including purfalcamine, melatonin derivative (**A** or N-[2-(1H-indol-3-yl)ethyl]hexanamide), and a series of inhibitors identified by an *in vitro* biochemical screening approach against chemical libraries of small molecules [23–26]. Compound **A** exhibited promising *in vitro* anti-parasitic activity [26]. Triazole-linked chalcone (**B**) [18], CQ-triazole-linked chalcones (**C**) [15], and indole-triazole hybrids (**D**) [19] were developed and evaluated for their antiplasmodial activity, whereas the indole-containing indolizine **A** was studied for its *Pf*CDPK1 inhibition (Fig. 1). Several other research groups have also contributed to this field [15,16,20,27].

Based on these active pharmacophore units namely quinoline, triazole, indole, and chalcones, we have successfully designed and developed side chain containing novel anti-malarial CQTrICh-analogs ((**7a-s** and **9**), exploring their potential *Pf*CDPK1-inhibitory effects. Here, we report the synthesis, characterization, physicochemical properties, and dose-dependent *in vitro* antimalarial activity against the chloroquine-sensitive (CQ^{S}) 3D7 strain of *P. falciparum*. However, two selective analogs (**7l** and **7r**) were evaluated for their anti-plasmodial activity against both *P. falciparum* CQ^{S}-3D7 as well as chloroquine-resistant (CQ^{R}) RKL-9, *Pf*CDPK1 inhibition, hematin inhibition, growth progression analysis, cytotoxic properties, and molecular docking studies. RKL-9 is a chloroquine-resistant and laboratory-adapted field isolate of *P. falciparum*, collected from a patient residing in the malaria endemic region of Orissa [28–31]. Overall, **7l** and **7r** exhibited promising results in antimalarial activity against both strains and were identified as *Pf*CDPK1 kinase inhibitors. This study opens the door to developing more bioisosteres for *Pf*CDPK1 kinase inhibitors.

2. Material and methods

2.1. Chemistry

2.1.1. Experimental protocols

All the chemical reagents and analytical grade solvents were purchased from Sigma-Aldrich, USA. Thin-layer chromatographic analysis was performed on pre-coated silica gel 60 F$_{254}$ TLC aluminium (Merck) sheets, and spots were visualized under 254 nm UV light. Only major peaks in cm^{-1} are provided for IR spectra collected on an Agilent Cary 630 FT-IR spectrometer. ^{1}H and ^{13}C NMR spectra were obtained with DMSO-d_6 as a solvent and tetramethylsilane (TMS) as an internal standard on a Bruker Spectrospin DPX-700 spectrometer at 700 MHz and 75 MHz, respectively. The following are the splitting patterns: s (singlet), d (doublet), t (triplet), m (multiplet) or brs (broad). The values of ^{1}H NMR chemical shifts (δ) are provided in parts per million (ppm) relative to residual solvent (DMSO-d_6, δ 2.54), and ^{13}C NMR chemical shifts (δ) are reported in ppm relative to (DMSO-d_6, δ 39.5) and coupling constants (J) are indicated in Hertz (Hz). An Agilent Quadrupole-6150 LC/MS spectrometer was used to collect mass spectra. Melting points were determined using an uncorrected digital Buchi melting point apparatus (M − 560). Purities were measured using an X-bridge C18 1.7 μm column (50 mm × 2.1 mm) with an Agilent RRLC MS 6320 ion trap spectrometer. The mobile phase channel A was made up of 5 mM ammonium acetate in water. Mobile phase B was acetonitrile at a flow rate of 0.8 mL/min; detection was accomplished with UV (214 nm), and all final compounds were found to be ≥ 95 % pure. The compounds were purified using silica gel column chromatography (230–400 mesh size) with the specified eluent.

2.1.2. Synthesis of chalcone (3a-s)

In a dried two-neck round bottom flask purged with argon, Indole 3-aldehyde **1** (1.0 mmol) was dissolved in anhydrous ethanol (10 ml). To this solution, substituted ketone **2a-s** (1.0 mmol) and piperidine (3.0 mmol) were added with constant stirring. The reaction mixture was then allowed to reflux for 24 h. A yellow precipitate formed during the course of the reaction was filtered and washed with chilled ethanol, dried, and recrystallized from ethanol to afford pure product [32]. All the chalcones were reported earlier [33–35].

2.1.3. Synthesis of alkyne (4a-s), (8)

At room temperature (RT), potassium carbonate (1.2 g, 8.55 mmol) was added to a solution of indole-chalcone (**3a-s**) or indole-3carboxaldehyde (**1**) (1.0 g, 3.42 mmol) in anhydrous DMF (10 ml). The reaction mixture was allowed to stir for 15 min at RT. Propargyl bromide (0.76 mL, 6.84 mmol) was added dropwise to this solution at RT. Under argon, the reaction mixture was agitated overnight. After the reaction was completed, the reaction mixture was quenched with water. Ethyl acetate (2 × 30 mL) was used to extract the aqueous phase. The mixed organic layers were washed with brine, dried over anhydrous sodium sulfate, and vacuum evaporated. As a result, the crude was extracted as intermediates **4a-s** (from **3a-s**) and **8** (from compound **1**). Finally, the crude was purified by column chromatography using 30 % ethyl acetate in hexane to obtain good to excellent yields of indole-chalcone alkyne [36].

2.1.3.1. (E)-1-phenyl-3-(1-(prop-2-yn-1-yl)-1H-indol-3-yl)prop-2-en-1-one (4a). Yellow solid, yield: 40.4 %, R_f = 0.75 (Ethylacetate: Hexane = 50 : 50), mp: 226.5 °C, IR (neat): ν (cm^{-1}) 3222 ($\equiv$C–H)$_{str}$, 1641 (C=C)$_{str}$. chalcone, ^{1}H NMR (700 MHz, DMSO-d_6) (δ-ppm): 8.20 (s, 1H, Ar–H), 8.14 (d, J = 7.2 Hz, 3H, CH, Ar–H), 8.03 (d, J = 15.5 Hz, 1H, Ar–H), 7.70 (d, J = 15.5 Hz, 1H, CH), 7.67–7.65 (m, 2H, Ar–H), 7.58 (t, J = 7.6 Hz, 2H, Ar–H), 7.36 (t, J = 7.5 Hz, 1H, Ar–H), 7.32 (d, J = 7.8 Hz, 1H, Ar–H), 5.20 (d, J = 2.5 Hz, 2H, CH$_2$), 3.53 (t, J = 2.5 Hz, $\equiv$C–H). ^{13}C NMR (176 MHz, DMSO-d_6) (δ-ppm): 188.81, 138.32, 138.02, 136.91, 134.92, 132.52, 128.75, 128.71, 128.18, 125.81, 123.04, 121.76, 120.70, 116.27, 112.58, 111.11, 78.39, 76.40, 35.67. ESI-MS (m/z) calcd. for C$_{20}$H$_{15}$N0: 285.34; Found: 286.16 [M+H]$^+$.

2.1.3.2. (E)-1-(2-nitrophenyl)-3-(1-(prop-2-yn-1-yl)-1H-indol-3-yl)prop-2-en-1-one (4b). Yellow solid, yield: 42.1 %, R_f = 0.73 (Ethylacetate: Hexane = 50 : 50) mp: 150.1 °C, IR (neat): ν (cm^{-1}) 3252 ($\equiv$C–H)$_{str}$, 1620 (C=C)$_{str}$. chalcone, ^{1}H NMR (700 MHz, DMSO-d_6) (δ, ppm): 8.18 (dd, J = 8.2, 0.9 Hz, 1H, CH), 8.11 (s, 1H, Ar–H), 7.99 (d, J = 8.0 Hz, 1H, C–H), 7.90 (td, J = 7.5, 1.1 Hz, 1H, Ar–H), 7.80 (td, J = 8.2, 1.4 Hz, 1H, Ar–H), 7.75 (dd, J = 7.5, 1.3 Hz, 1H, Ar–H), 7.66 (t, J = 11.8 Hz, 2H, Ar–H), 7.36–7.33 (m, 1H, Ar–H), 7.29–7.26 (m, 1H, Ar–H), 7.09 (d, J = 16.1 Hz, 1H, Ar–H), 5.17 (d, J = 2.5 Hz, 2H, CH$_2$), 3.52 (t, J = 2.5 Hz, 1H, $\equiv$CH). ^{13}C NMR (176 MHz, DMSO-d_6) (δ-ppm): 191.51, 147.06, 140.50, 136.97, 135.91, 135.66, 134.07, 131.00, 129.10, 125.45, 124.44, 123.18, 121.95, 120.57, 119.98, 111.90, 111.21, 78.19, 76.50, 35.70. ESI-MS (m/z) calcd. for C$_{20}$H$_{14}$N$_2$O$_3$: 330.34; Found: 331.04 [M+H]$^+$.

2.1.3.3. (E)-1-(3-nitrophenyl)-3-(1-(prop-2-yn-1-yl)-1H-indol-3-yl)prop-2-en-1-one (4c). Yellow solid, yield: 40.1 %, R_f = 0.75 (Ethylacetate: Hexane = 50 : 50) mp: 200.1 °C, IR (neat): ν (cm^{-1}) 3235 ($\equiv$C–H)$_{str}$, 1641 (C=C)$_{str}$. chalcone ^{1}H NMR (700 MHz, DMSO-d_6) (δ, ppm): 8.78–8.77 (m, 1H), 8.63–8.61 (m, 1H, Ar–H), 8.49 (ddd, J = 8.1, 2.3, 0.9 Hz, 1H, Ar–H), 8.28 (s, 1H, Ar–H), 8.18 (d, J = 7.8 Hz, 1H, Ar–H), 8.13 (d, J = 15.4 Hz, 1H, Ar–H), 7.89 (t, J = 7.9 Hz, 1H, Ar–H), 7.74 (d, J = 15.4 Hz, 1H, Ar–H), 7.67 (d, J = 8.1 Hz, 1H, Ar–H), 7.39–7.36 (m, 1H, Ar–H), 7.35–7.32 (m, 1H, Ar–H), 5.22 (d, J = 2.5 Hz, 2H, CH$_2$), 3.55 (t, J = 2.5 Hz, $\equiv$C–H). ^{13}C NMR (176 MHz, DMSO-d_6) (δ-ppm): 187.47, 148.66, 140.09, 137.43, 136.11, 134.96, 131.00, 127.18, 126.30, 123.67, 122.40, 121.24, 115.95, 113.12, 111.69, 87.73, 78.77, 77.01, 36.24., ESI-MS (m/z) calcd. for C$_{20}$H$_{14}$N$_2$O$_3$: 330.34; Found: 331.08 [M+H]$^+$.

2.1.3.4. (E)-1-(4-nitrophenyl)-3-(1-(prop-2-yn-1-yl)-1H-indol-3-yl)prop-2-en-1-one (4d). Yellow solid, yield: 89.1 %, R_f = 0.75 (Ethylacetate: Hexane = 50 : 50), mp: 189.8 °C, IR (neat): ν (cm^{-1}) 3267 ($\equiv$C–H)$_{str}$, 1654 (C=C)$_{str}$. chalcone, ^{1}H NMR (700 MHz, DMSO-d_6) (δ, ppm): 8.37 (dd, J = 22.9, 8.9 Hz, 2H, Ar–H), 8.26 (s, 1H, Ar–H), 8.18 (d, J = 7.8 Hz, 1H, CH), 8.10 (d, J = 15.4 Hz, 1H, Ar–H), 7.75 (d, J = 15.2 Hz, 3H, Ar–H), 7.68 (t, J = 11.3 Hz, 2H, CH), 7.35 (t, J = 7.9 Hz, 2H, Ar–H), 5.22 (d, J = 2.5 Hz, 1H, Ar–H), 3.55 (t, J = 2.5 Hz, $\equiv$C–H). ^{13}C NMR (176 MHz, DMSO-d_6) (δ-ppm): 188.25, 149.95, 143.86, 140.23, 137.48, 136.37, 130.03, 126.21, 124.29, 123.71, 122.45, 121.32, 116.36, 113.12, 111.71, 78.74, 77.03, 36.24. ESI-MS (m/z) calcd. for C$_{20}$H$_{14}$N$_2$O$_3$: 330.3; Found: 331.17 [M+H]$^+$.

2.1.3.5. (E)-1-(2-bromophenyl)-3-(1-(prop-2-yn-1-yl)-1H-indol-3-yl)prop-2-en-1-one (4e). Yellow solid, yield: 76.9 %, R_f = 0.78 (Ethylacetate: Hexane = 50 : 50),mp: 90.1 °C, IR (neat): ν (cm^{-1}) 3278 ($\equiv$C–H)$_{str}$, 1663 (C=C)$_{str}$. chalcone, ^{1}H NMR (700 MHz, DMSO-d_6) (δ, ppm): 8.12 (s, 1H, Ar–H), 7.96 (d, J = 7.9 Hz, 1H, CH), 7.75 (dd, J = 8.0, 0.7 Hz, 1H, Ar–H), 7.65 (d, J = 8.2 Hz, 1H, CH), 7.59 (d, J = 16.0 Hz, 1H, Ar–H), 7.52 (dd, J = 4.7, 1.5 Hz, 1H, Ar–H), 7.46 (dd, J = 2.1, 1.0 Hz, 1H, Ar–H), 7.35 (t, J = 7.2 Hz, 1H, Ar–H), 7.28 (t, J = 7.1 Hz, 1H, Ar–H), 7.04 (d, J = 16.0 Hz, 1H, Ar–H), 5.16 (d, J = 2.4 Hz, 2H, CH$_2$), 3.51 (t, J = 2.5 Hz, $\equiv$C–H). ^{13}C NMR (176 MHz, DMSO-d_6) (δ-ppm): 193.78, 141.50, 140.78, 137.00, 135.62, 133.02, 131.29, 129.00, 127.79, 125.49, 123.19, 122.02, 120.79, 120.44, 118.63, 111.99, 111.26, 78.21, 76.47, 35.71. ESI-MS (m/z) calcd. for C$_{20}$H$_{14}$BrNO: 364.2; Found: 366.10 [M+2H]$^+$.

2.1.3.6. (E)-1-(3-bromophenyl)-3-(1-(prop-2-yn-1-yl)-1H-indol-3-yl)prop-2-en-1-one (4f). Yellow solid, yield: 45 %, R_f = 0.78 (Ethylacetate: Hexane = 50 : 50), mp: 148 °C, IR (neat): ν (cm^{-1}) 3235 ($\equiv$C–H)$_{str}$, 1641 (C=C)$_{str}$. chalcone, ^{1}H NMR (700 MHz, DMSO-d_6) (δ, ppm): 8.24 (dd, J = 4.5, 2.7 Hz, 2H, Ar–H), 8.16 (t, J = 7.0 Hz, 2H, Ar–H), 8.06 (d, J = 15.3 Hz, 1H, CH), 7.86–7.85 (m, 1H, Ar–H), 7.66 (dd, J = 7.9, 3.4 Hz, 2H, Ar–H), 7.56–7.53 (m, 1H, Ar–H), 7.37–7.35 (m, 1H, Ar–H), 5.31 (d, J = 2.5 Hz, 1H, Ar–H), 5.21 (d, J = 2.5 Hz, 2H, CH$_2$), 3.54 (t, J = 2.5 Hz, 1H, $\equiv$C–H). ^{13}C NMR (176 MHz, DMSO-d_6) (δ-ppm): 187.45, 140.43, 138.79, 136.89, 135.64, 135.16, 135.11, 134.89, 134.75, 131.02, 130.95, 130.58, 130.46, 127.29, 126.91, 125.86, 123.10, 122.23, 121.82, 121.42, 120.72, 118.28, 115.74, 114.95, 112.61, 111.11, 110.97, 78.33, 76.50, 76.46, 35.71. ESI-MS (m/z) calcd. for C$_{20}$H$_{14}$BrNO: 364.2; Found: 366.09 [M+H]$^+$.

2.1.3.7. (E)-1-(4-bromophenyl)-3-(1-(prop-2-yn-1-yl)-1H-indol-3-yl)prop-2-en-1-one (4g). Yellow solid, yield: 44.4 %, R_f = 0.75

(Ethylacetate: Hexane = 50 : 50), mp: 193.5 °C, IR (neat): ν (cm^{-1}) 3227 ($\equiv$C–H)$_{str}$, 1642 (C=C)$_{str}$ chalcone, ^{1}H NMR (700 MHz, DMSO-d_6) (δ, ppm): 8.22 (s, 1H, Ar–H), 8.15 (d, J = 7.9 Hz, 1H, Ar–H), 8.10–8.08 (m, 2H, Ar–H), 8.05 (d, J = 15.4 Hz, 1H, Ar–H), 8.02–8.00 (m, 1H, Ar–H), 7.79–7.76 (m, 3H, Ar–H), 7.65 (t, J = 7.5 Hz, 2H, Ar–H), 5.21 (d, J = 2.5 Hz, 2H, CH_2), 3.53 (t, J = 2.5 Hz, 1H, $\equiv$C–H). ^{13}C NMR (176 MHz, DMSO-d_6) (δ-ppm): 188.37, 188.30, 139.05, 137.78, 137.40, 135.97, 135.78, 135.69, 135.13, 132.25, 132.20, 130.75, 130.45, 126.98, 126.25, 123.57, 122.28, 121.84, 121.23, 118.75, 116.26, 115.53, 113.07, 111.61, 78.81, 76.92, 36.17. ESI-MS (*m/z*) calcd. for C$_{20}$H$_{14}$BrN0: 364.24; Found: 364.08 [M+H]$^+$.

2.1.3.8. (E)-1-(2-chlorophenyl)-3-(1-(prop-2-yn-1-yl)-1H-indol-3-yl)prop-2-en-1-one (4h). Yellow solid, yield: 84.2 %, R$_f$ = 0.75 (Ethylacetate: Hexane = 50 : 50), mp: 95.1 °C, IR (neat): ν (cm^{-1}) 3261 ($\equiv$C–H)$_{str}$, 1646 (C=C)$_{str}$ chalcone, ^{1}H NMR (700 MHz, DMSO-d_6) (δ, ppm): 8.12 (s, 1H, Ar–H), 7.96 (d, J = 7.9 Hz, 1H, CH), 7.65 (d, J = 9.5 Hz, 2H, CH), 7.59 (d, J = 9.0 Hz, 1H, Ar–H), 7.56 (d, J = 7.8 Hz, 2H, Ar–H), 7.49 (t, J = 6.8 Hz, 1H, Ar–H), 7.35 (t, J = 7.2 Hz, 1H, Ar–H), 7.28 (t, J = 7.5 Hz, 1H, Ar–H), 7.07 (d, J = 16.0 Hz, 1H, Ar–H), 5.17 (d, J = 2.4 Hz, 2H, CH_2), 3.51 (t, J = 2.5 Hz, 1H, $\equiv$C–H). ^{13}C NMR (176 MHz, DMSO-d_6) (δ-ppm): 193.29, 141.04, 139.94, 137.48, 136.11, 131.76, 130.44, 130.28, 129.61, 127.82, 125.98, 123.66, 122.49, 121.45, 120.92, 112.45, 111.74, 78.70, 76.96, 36.19. ESI-MS (*m/z*) calcd. for C$_{20}$H$_{14}$ClN0: 319.8; Found: 320.13 [M+H]$^+$.

2.1.3.9. (E)-1-(3-chlorophenyl)-3-(1-(prop-2-yn-1-yl)-1H-indol-3-yl)prop-2-en-1-one (4i). Yellow solid, yield: 76.51 %, R$_f$ = 0.75 (Ethylacetate: Hexane = 50 : 50), mp: 144.6 °C, IR (neat): ν (cm^{-1}) 3291 ($\equiv$C–H)$_{str}$, 1652 (C=C)$_{str}$ chalcone, ^{1}H NMR (700 MHz, DMSO-d_6) (δ, ppm): 8.25 (s, 1H, Ar–H), 8.16 (d, J = 7.8 Hz, 1H, CH), 8.13–8.12 (m, 2H, Ar–H), 8.06–8.05 (m, 1H, Ar–H), 7.95 (d, J = 7.9 Hz, 1H, CH), 7.66 (dd, J = 8.5, 3.3 Hz, 2H, Ar–H), 7.33–7.32 (m, 1H, Ar–H), 7.04 (d, J = 12.3 Hz, 1H, Ar–H), 5.21 (d, J = 2.5 Hz, 2H, CH$_2$), 3.54 (t, J = 2.5 Hz, 1H, $\equiv$C–H). ^{13}C NMR (176 MHz, DMSO-d_6) (δ-ppm): ^{13}C NMR (176 MHz, DMSO-d_6) (δ-ppm): 187.98, 140.72, 139.29, 137.38, 135.68, 134.19, 132.70, 131.18, 128.20, 127.39, 126.33, 123.58, 122.30, 121.23, 118.76, 116.24, 113.09, 111.59, 78.84, 76.95, 36.20. ESI-MS (*m/z*) calcd. for C$_{20}$H$_{14}$ClNO: 319.18; Found: 320.11 [M+H]$^+$.

2.1.3.10. 2.1.3.10(E)-1-(4-chlorophenyl)-3-(1-(prop-2-yn-1-yl)-1H-indol-3-yl)prop-2-en-1-one (4j). Yellow solid, yield: 57.8 %, R$_f$ = 0.75 (Ethylacetate: Hexane = 50 : 50), mp: 192.1 °C, IR (neat): ν (cm^{-1}) 3267 ($\equiv$C–H)$_{str}$, 1652 (C=C)$_{str}$ chalcone, ^{1}H NMR (700 MHz, DMSO-d_6) (δ, ppm): 8.22 (s, 1H, Ar–H), 8.18–8.16 (m, 2H, Ar–H), 8.10–8.08 (m, 1H, Ar–H), 8.05 (d, J = 15.4 Hz, 1H, CH), 7.69 (s, 1H, Ar–H), 7.66 (d, J = 8.6 Hz, 2H, CH), 7.64 (d, J = 1.8 Hz, 1H, Ar–H), 7.63 (d, J = 2.0 Hz, 1H, Ar–H), 7.36 (t, J = 7.1 Hz, 1H, Ar–H), 5.21 (d, J = 2.5 Hz, 2H, CH$_2$), 3.53 (t, J = 2.5 Hz, 1H, $\equiv$C–H). ^{13}C NMR (176 MHz, DMSO-d_6) (δ-ppm): 187.63, 138.55, 137.38, 136.98, 136.93, 135.28, 135.21, 134.64, 130.14, 129.84, 128.83, 128.78, 125.78, 123.10, 121.80, 121.36, 120.76, 118.28, 115.81, 115.12, 112.60, 111.13, 110.94, 78.35, 76.45, 35.70. ESI-MS (*m/z*) calcd. for C$_{20}$H$_{14}$ClN0: 319.8; Found: 320.11 [M+H]$^+$.

2.1.3.11. (E)-1-(2,4-dichlorophenyl)-3-(1-(prop-2-yn-1-yl)-1H-indol-3-yl)prop-2-en-1-one (4k). Yellow solid, yield: 56.3 %, R$_f$ = 0.75 (Ethylacetate: Hexane = 50 : 50), mp: 147.9 °C, IR (neat): ν (cm^{-1}) 3283 ($\equiv$C–H)$_{str}$, 1648 (C=C)$_{str}$ chalcone, ^{1}H NMR (700 MHz, DMSO-d_6) (δ, ppm): 8.14 (s, 1H, Ar–H), 7.98 (d, J = 8.0 Hz, 1H, CH), 7.78 (d, J = 1.6 Hz, 1H, CH), 7.67–7.64 (m, 2H, Ar–H), 7.59–7.58 (m, 2H, Ar–H), 7.35 (t, J = 8.1 Hz, 1H, Ar–H), 7.28 (t, J = 7.5 Hz, 1H, Ar–H), 7.05 (d, J = 16.0 Hz, 1H, Ar–H), 5.17 (d, J = 2.5 Hz, 2H, CH_2), 3.52 (t, J = 2.5 Hz, 1H, $\equiv$C–H). ^{13}C NMR (176 MHz, DMSO-d_6) (δ-ppm): 192.43, 141.71, 138.75, 137.47, 136.37, 135.42, 131.56, 131.02, 130.00, 128.08, 125.97, 123.71, 122.52, 121.17, 121.04, 112.53, 111.76, 78.66, 77.03, 36.22. ESI-MS (*m/z*) calcd. for C$_{20}$H$_{13}$Cl$_2$NO: 354.2; Found: 356.21 [M+H]$^+$.

2.1.3.12. (E)-1-(2-methoxyphenyl)-3-(1-(prop-2-yn-1-yl)-1H-indol-3-yl)prop-2-en-1-one (4l). Cream solid, yield: 48 %, R$_f$ = 0.78 (Ethylacetate: Hexane = 50 : 50), mp: 109 °C, IR (neat): ν (cm^{-1}) 3296 ($\equiv$C–H)$_{str}$, 1655 (C=C)$_{str}$ chalcone, ^{1}H NMR (700 MHz, DMSO-d_6) (δ, ppm): 8.37 (s, 1H, Ar–H), 8.13 (d, J = 7.8 Hz, 1H, CH), 7.67 (d, J = 8.2 Hz, 1H, CH), 7.38–7.36 (m, 1H, Ar–H), 7.32–7.29 (m, 3H, Ar–H), 5.26 (d, J = 2.5 Hz, 2H, CH$_2$), 3.57 (t, J = 2.5 Hz, 1H, $\equiv$C–H), 3.33 (s, 6H, CH$_3$). ^{13}C NMR (176 MHz, DMSO-d_6) (δ-ppm): 184.92, 140.15, 136.58, 124.68, 123.73, 122.79, 121.12, 117.55, 111.22, 78.01, 76.83, 36.02. ESI-MS (*m/z*) calcd. for C$_{21}$H$_{17}$NO$_2$: 315.4; Found: 314.97 [M – H]$^+$.

2.1.3.13. (E)-1-(3-methoxyphenyl)-3-(1-(prop-2-yn-1-yl)-1H-indol-3-yl)prop-2-en-1-one (4 m). Yellow solid, yield: 61.05 %, R$_f$ = 0.75 (Ethylacetate: Hexane = 50 : 50), mp: 118.7 °C, IR (neat): ν (cm^{-1}) 3259 ($\equiv$C–H)$_{str}$, 1646 (C=C)$_{str}$ chalcone, ^{1}H NMR (700 MHz, DMSO-d_6) (δ, ppm): 8.37 (s, 1H, Ar–$H)$, 8.21 (s, 1H, Ar–H), 8.13 (d, J = 7.9 Hz, 1H, CH), 8.03 (d, J = 15.5 Hz, 1H, Ar–H), 7.75 (d, J = 7.7 Hz, 1H, CH), 7.66 (d, J = 5.6 Hz, 2H, Ar–H), 7.36 (d, J = 8.3 Hz, 1H, Ar–H), 7.23 (dd, J = 7.9, 2.3 Hz, 1H, Ar–H), 5.26 (d, J = 2.4 Hz, 2H), 5.20 (d, J = 2.4 Hz, 2H), 3.86 (d, J = 6.6 Hz, 3H, CH$_3$), 3.57 (t, J = 2.1 Hz, 1H, $\equiv$C–H). ^{13}C NMR (176 MHz, DMSO-d_6) (δ-ppm): 188.57, 184.92, 159.49, 140.14, 139.84, 138.01, 136.88, 136.57, 134.82, 129.85, 124.68, 123.73, 123.02, 122.79, 121.76, 121.12, 120.69, 120.62, 118.45, 117.55, 116.39, 112.72, 112.55, 111.226, 111.10, 76.83, 76.40, 55.31, 36.01, 35.67. ESI-MS (*m/z*) calcd. for C$_{21}$H$_{17}$NO$_2$: 315.4; Found: 316.16 [M+H]$^+$.

2.1.3.14. (E)-1-(4-methoxyphenyl)-3-(1-(prop-2-yn-1-yl)-1H-indol-3-yl)prop-2-en-1-one (4n). Yellow solid, yield: 36.6 %, R$_f$ = 0.80 (Ethylacetate: Hexane = 50 : 50), mp: 179.3 °C, IR (neat): ν (cm^{-1}) 3235 ($\equiv$C–H)$_{str}$, 1642 (C=C)$_{str}$ chalcone. ^{1}H NMR (700 MHz, DMSO-d_6) (δ, ppm): 8.17 (s, 1H, Ar–H), 8.15 (d, J = 8.9 Hz, 2H, Ar–H), 8.13 (d, J = 7.8 Hz, 1H, CH), 7.99 (d, J = 15.4 Hz, 1H, CH), 7.70 (d, J = 15.5 Hz, 1H, Ar–H), 7.65 (d, J = 8.1 Hz, 1H, Ar–H), 7.35 (t, J = 7.5 Hz, 1H, Ar–H), 7.31 (t, J = 7.4 Hz, 1H, Ar–H), 7.10 (t, J = 5.8 Hz, 2H, Ar–H), 5.20 (d, J = 2.4 Hz, 2H, CH_2), 3.88 (s, 3H, CH$_3$), 3.52 (t, J = 2.5 Hz, 1H, $\equiv$C–H). ^{13}C NMR (176 MHz, DMSO-d_6) (δ-ppm):

187.63, 163.24, 137.53, 137.36, 134.92, 131.58, 130.99, 130.70, 126.34, 123.44, 122.12, 121.14, 116.76, 114.40, 113.08, 111.54, 78.92, 76.83, 55.98, 36.11. ESI-MS (*m/z*) calcd. for $C_{21}H_{17}NO_2$: 315.37; Found: 316.15 $[M+H]^+$.

2.1.3.15. (E)-1-(3,4-dimethoxyphenyl)-3-(1-(prop-2-yn-1-yl)-1H-indol-3-yl)prop-2-en-1-one (4o). Yellow solid, yield: 35.4 %, $R_f = 0.80$ (Ethylacetate: Hexane = 50 : 50), mp: 173.8 °C, IR (neat): ν (cm^{-1}) 3259 ($\equiv$C–H)$_{str}$, 1642 (C=C)$_{str.}$ chalcone. ^{1}H NMR (700 MHz, DMSO-d_6) (δ, ppm): 8.18 (s, 1H, Ar–*H*), 8.12 (d, *J* = 7.8 Hz, 1H, C*H*), 7.99 (d, *J* = 15.4 Hz, 1H, C*H*), 7.88 (dd, *J* = 8.4, 2.0 Hz, 1H, Ar–*H*), 7.71 (d, *J* = 15.5 Hz, 1H, Ar–*H*), 7.65 (d, *J* = 8.1 Hz, 1H, Ar–*H*), 7.60 (d, *J* = 1.9 Hz, 1H, Ar–*H*), 7.35 (t, *J* = 7.5 Hz, 1H, Ar–*H*), 7.31 (t, *J* = 7.0 Hz, 1H, Ar–*H*), 7.12 (d, *J* = 8.4 Hz, 1H, Ar–*H*), 5.20 (d, *J* = 2.4 Hz, 2H, C*H₂*), 3.88 (d, *J* = 6.1 Hz, 6H, C*H₃*), 3.52 (t, *J* = 2.5 Hz, 1H, $\equiv$C–*H*). ^{13}C NMR (176 MHz, DMSO-d_6) (δ-ppm): 187.68, 153.19, 149.22, 137.36, 137.31, 134.74, 131.66, 126.38, 123.41, 123.22, 122.10, 121.04, 116.80, 113.07, 111.50, 111.34, 111.08, 78.94, 76.82, 56.21, 56.02, 36.11. ESI-MS (*m/z*) calcd. for $C_{22}H_{19}NO_3$: 345.39; Found: 346.14 $[M+H]^+$.

2.1.3.16. (E)-3-(1-(prop-2-yn-1-yl)-1H-indol-3-yl)-1-(thiophen-2-yl)prop-2-en-1-one (4p). Yellow solid, yield: 42.9 %, $R_f = 0.75$ (Ethylacetate: Hexane = 50 : 50), mp: 162.4 °C, IR (neat): ν (cm^{-1}) 3270 ($\equiv$C–H)$_{str}$, 1642 (C=C)$_{str.}$ chalcone, ^{1}H NMR (700 MHz, DMSO-d_6) (δ, ppm): 8.28 (dd, *J* = 3.8, 1.0 Hz, 1H, Ar–*H*), 8.19–8.17 (m, 2H, Ar–H,C*H*), 8.01 (dd, *J* = 4.1, 1.8 Hz, 1H, Ar–*H*), 7.99–7.98 (m, 1H,C*H*), 7.67–7.63 (m, 2H, Ar–*H*), 7.61 (s, 1H, Ar–*H*), 7.37–7.35 (m, 1H, Ar–*H*), 7.32 (dd, *J* = 5.9, 2.2 Hz, 1H, Ar–*H*), 7.28–7.27 (m, 1H, Ar–*H*), 5.20 (s, 1H, Ar–*H*), 3.53 (d, *J* = 2.5 Hz, 1H, $\equiv$C–*H*). ^{13}C NMR (176 MHz, DMSO-d_6) (δ-ppm): 181.60, 181.41, 147.07, 146.10, 137.12, 136.89, 135.44, 134.95, 134.81, 134.46, 134.35, 134.18, 132.35, 131.53, 128.84, 128.75, 125.76, 123.04, 122.72, 121.73, 121.30, 120.79, 118.22, 116.02, 115.08, 112.39, 111.07, 110.89, 78.37, 76.40, 35.66. ESI-MS (*m/z*) calcd. for $C_{18}H_{13}NOS$: 291.4; Found: 292.11 $[M+H]^+$.

2.1.3.17. (E)-1-(3,5-bis(benzyloxy)phenyl)-3-(1-(prop-2-yn-1-yl)-1H-indol-3-yl)prop-2-en-1-one (4q). Yellow solid, yield: 55.3 %, $R_f = 0.75$ (Ethylacetate: Hexane = 50 : 50), mp: 147.0 °C, IR (neat): ν (cm^{-1}) 3278 ($\equiv$C–H)$_{str}$, 1654 (C=C)$_{str.}$ chalcone. ^{1}H NMR (700 MHz, DMSO-d_6) (δ, ppm): 8.37 (s, 1H, Ar–*H*), 8.22 (s, 3H, Ar–*H*), 8.07 (d, *J* = 7.7 Hz, 2H, Ar–H, C*H*), 8.01 (d, *J* = 15.4 Hz, 2H, Ar–*H*), 7.65 (d, *J* = 8.1 Hz, 3H, Ar–H, C*H*), 7.58 (d, *J* = 15.5 Hz, 3H, Ar–*H*), 7.18 (s, 1H, Ar–*H*), 6.97 (d, *J* = 2.2 Hz, 3H, Ar–*H*), 5.30 (s, 1H, Ar–*H*), 5.26 (d, *J* = 2.5 Hz, 1H, Ar–*H*), 5.17 (s, 3H,C*H₂*, Ar–*H*), 5.11 (s, 1H, Ar–*H*), 3.53 (s, 3H, Ar–H, $\equiv$C–*H*). ^{13}C NMR (176 MHz, DMSO-d_6) (δ-ppm): 188.76, 185.40, 160.12, 160.06, 141.00, 138.54, 137.32, 137.18, 135.14, 128.95, 128.40, 128.27, 126.40, 124.21, 123.49, 123.28, 122.23, 121.60, 121.00, 116.76, 113.02, 111.71, 111.56, 107.57, 107.50, 106.46, 78.85, 77.31, 76.89, 70.05, 36.17. ESI-MS (*m/z*) calcd. for $C_{34}H_{27}NO_3$: 497.6; Found: 498.21 $[M+H]^+$.

2.1.3.18. (E)-3-(1-(prop-2-yn-1-yl)-1H-indol-3-yl)-1-(o-tolyl)prop-2-en-1-one (4r). Yellow solid, yield: 34.4 %, $R_f = 0.75$ (Ethylacetate: Hexane = 50 : 50), mp: 221.5 °C, IR (neat): ν (cm^{-1}) 3221 ($\equiv$C–H)$_{str}$, 1643 (C=C)$_{str.}$ chalcone. ^{1}H NMR (700 MHz, DMSO-d_6) (δ-ppm): 8.10 (s, 1H, Ar–*H*), 8.12 (d, *J* = 7.1 Hz, 2H, CH, Ar–*H*), 8.03 (d, *J* = 15.5 Hz, 2H,Ar–*H*), 7.73 (d, *J* = 15.1 Hz, 1H, C*H*), 7.61–7.69 (m, 1H, Ar–*H*), 7.46 (t, *J* = 7.4 Hz, 2H, Ar–*H*), 7.33 (t, *J* = 7.2 Hz, 1H, Ar–*H*), 7.31 (d, *J* = 7.7 Hz, 1H, Ar–*H*), 5.22 (d, *J* = 2.4 Hz, 2H, C*H₂*), 3.53 (t, *J* = 2.5 Hz, 1H, $\equiv$C–*H*), 2.12 (s, 3H, C*H₃*). ^{13}C NMR (176 MHz, DMSO-d_6) (δ-ppm): 188.51, 138.33, 138.21, 135.53, 134.12, 133.51, 129.45, 128.41, 128.12, 125.31, 124.44, 121.75, 120.52, 116.25, 112.57, 112.01, 78.32, 76.40, 35.77. ESI-MS (*m/z*) calcd. for $C_{21}H_{17}NO$: 299.37; Found: 300.52 $[M+H]^+$.

2.1.3.19. (E)-1-(4-fluorophenyl)-3-(1-(prop-2-yn-1-yl)-1H-indol-3-yl)prop-2-en-1-one (4s). Yellow solid, yield: 66.7 %, $R_f = 0.75$ (Ethylacetate: Hexane = 50 : 50), mp: 168.6 °C, IR (neat): ν (cm^{-1}) 3265 ($\equiv$C–H)$_{str}$, 1652 (C=C)$_{str.}$ chalcone. ^{1}H NMR (700 MHz, DMSO-d_6) (δ, ppm): 8.24 (dd, *J* = 8.8, 5.6 Hz, 2H, Ar–*H*), 8.20 (s, 1H, Ar–*H*), 8.16 (d, *J* = 7.9 Hz, 1H, C*H*), 8.03 (d, *J* = 15.4 Hz, 1H, C*H*), 7.69 (d, *J* = 15.4 Hz, 1H, Ar–*H*), 7.66 (d, *J* = 8.2 Hz, 1H, Ar–*H*), 7.40 (t, *J* = 8.8 Hz, 2H, Ar–*H*), 7.37–7.35 (m, 1H, Ar–*H*), 7.31 (t, *J* = 7.1 Hz, 1H, Ar–*H*), 5.21 (d, *J* = 2.5 Hz, 2H, C*H₂*), 3.53 (t, *J* = 2.5 Hz, 1H, $\equiv$C–*H*). ^{13}C NMR (176 MHz, DMSO-d_6) (δ-ppm): 187.79, 165.88, 164.46, 138.67, 137.38, 135.49, 135.41, 135.36, 131.61, 131.56, 131.25, 126.27, 123.53, 122.22, 121.23, 116.40, 116.18, 116.06, 113.05, 111.58, 78.84, 76.89, 36.15. ESI-MS (*m/z*) calcd. for $C_{20}H_{14}FNO$: 303.3; Found: 304.23 $[M+H]^+$.

2.1.3.20. 1-(prop-2-yn-1-yl)-1H-indole-3-carbaldehyde (8). Cream solid, yield: 90.4 %, $R_f = 0.75$ (Ethylacetate: Hexane = 50 : 50), mp: 108.9 °C, IR (neat): ν (cm^{-1}) 3298 ($\equiv$C–H)$_{str}$, 1641 (C=C)$_{str.}$ chalcone, ^{1}H NMR (700 MHz, DMSO-d_6) (δ, ppm): 9.95 (s, 1H, CHO), 8.37 (s, 1H, Ar–*H*), 8.14 (d, *J* = 7.8 Hz, 1H, Ar–*H*), 7.67 (d, *J* = 8.2 Hz, 1H, Ar–*H*), 7.38–7.36 (m, 1H, Ar–*H*), 7.32–7.29 (m, 1H, Ar–*H*), 5.26 (d, *J* = 2.4 Hz, 2H, C*H₂*), 3.57 (t, *J* = 2.5 Hz, 1H, $\equiv$C–*H*). ^{13}C NMR (176 MHz, DMSO-d_6) (δ-ppm): 184.92, 140.15, 136.57, 124.68, 123.73, 122.79, 121.12, 117.55, 111.22, 78.00, 76.83, 36.01. ESI-MS (*m/z*) calcd. for $C_{12}H_9NO$: 183.21; Found: 184.34 $[M+H]^+$.

2.1.4. Synthesis of azide (6)

A solution of 4,7-dichloroquinoline (**5**) (1.0 mmol) in anhydrous DMF (5 ml) and sodium azide (6.0 mmol) were added to a dry round bottom flask and the reaction mixture was stirred at 85 °C for 3 h. After the reaction was completed, the mixture was poured into water, extracted with chloroform (2 × 30 mL), dried over sodium sulfate, and concentrated under vacuum to yield azide, which was then used further without purification [37].

2.1.5. General procedure for the synthesis of triazole hybrids (7a-s) and 9

In a dried round bottom flask, Indole-chalcone alkynes **4a-s**/indole alkyne **8** (0.20 g, 0.61 mmol) and azide **6** (0.093 g, 0.61 mmol)

were dissolved in a mixture of solvent system, THF/H$_2$O (1:2, 9 ml). After that, sodium ascorbate (0.063 g, 0.32 mmol) was added followed by the addition of CuSO$_4$.5H$_2$O (0.026 g, 0.11 mmol). The reaction mixture was stirred until all of the starting ingredients had disappeared. The obtained solid was filtered and rinsed with water to get pure compounds, the crude product was purified using silica gel chromatography and eluting with a solution of methanol (5 %) in dichloromethane [38].

2.1.5.1. (E)-3-(1-((1-(7-chloroquinolin-4-yl)-1H-1,2,3-triazol-4-yl)methyl)-1H-indol-3-yl)-1-phenylprop-2-en-1-one (7a). Yellow solid, yield: 62 %, R$_f$ = 0.69 (Methanol: dichloromethane = 5 : 95), mp: 225.1–225.3 °C, IR (neat): ν (cm^{-1}) 3152 (C–H)$_{str.}$ triazole ring, 1648 (C═C)$_{str.}$ chalcone, ^{1}H NMR (700 MHz, DMSO-d_6) (δ, ppm): 9.12 (t, J = 4.83 Hz, 1H, CQ-H), 8.94 (s, 1H, NC-H_{indole}), 8.32 (s, 1H, Ar–H), 8.28 (d, J = 2.03 Hz,1H, C-$H_{triazole}$), 8.13-8.11 (m, 3H, Ar–H), 8.05 (m, 1H, Ar–H), 7.98 (d, J = 9.17 Hz, 1H, Ar–H), 7.83-7.81 (m, 3H, Ar–H), 7.78 (d, J = 1.89 Hz, 1H, Ar–H), 7.68 (d, J = 15.5 Hz, 1H, Ar–H), 7.64 (s, 1H, Ar–H), 7.55-7.54 (m, 3H, Ar–H), 5.74 (s, 2H, CH_2). ^{13}C NMR (176 MHz, DMSO-d_6) (δ, ppm): 189.26, 152.83, 149.85, 143.92, 140.75, 138.83, 138.65, 137.71, 136.05, 135.84, 132.96, 129.47, 129.22, 129.18, 128.63, 128.38, 126.26, 126.33, 125.88, 123.49, 122.13, 121.14, 120.73, 117.67, 117.63, 116.51, 112.99, 111.77. ESI-MS (*m/z*) calcd. for C$_{29}$H$_{20}$ClN$_5$O: 489.96; Found: 462.24 [M-N$_2$+1]$^+$, 464.27 [M-N$_2$+2 + 1]$^+$, 465.30 [M-N$_2$+2 + 2]$^+$. Purity: UP-LC 91.04 %.

2.1.5.2. (E)-3-(1-((1-(7-chloroquinolin-4-yl)-1H-1,2,3-triazol-4-yl)methyl)-1H-indol-3-yl)-1-(2-nitrophenyl)prop-2-en-1-one (7b). Yellow solid, yield: 73 %, R$_f$ = 0.85 (Methanol: dichloromethane = 5 : 95), mp: 210.4–210.7 °C, IR (neat): ν (cm^{-1}) 3136 (C–H)$_{str.}$ triazole ring, 1611 (C═C)$_{str.}$ chalcone, ^{1}H NMR (700 MHz, DMSO-d_6) (δ, ppm): 9.11 (d, J = 4.69 Hz, 1H, CQ-H), 8.91 (s, 1H, NC-H_{indole}), 8.26 (d, J = 1.75 Hz, 1H, Ar–H), 8.22 (s, 1H, C-$H_{triazole}$), 8.15 (d, J = 8.19 Hz, 1H, Ar–H), 7.96 (t, J = 7.56 Hz, 2H, Ar–H), 7.87 (d, J = 14.98 Hz, 1H, Ar–H), 7.81 (t, J = 4.48 Hz, 2H, Ar–H), 7.76 (d, J = 9.66 Hz, 1H, Ar–H), 7.74 (d, J = 10.15 Hz, 2H, Ar–H), 7.66 (s, 1H, Ar–H), 7.30 (t, J = 7.56 Hz, 1H, Ar–H), 7.25 (t, J = 7.63 Hz, 1H, Ar–H), 7.07 (d, J = 16.1 Hz, 1H, Ar–H), 5.70 (s, 2H, CH_2). ^{13}C NMR (176 MHz, DMSO-d_6) (δ, ppm): 192.03, 152.81, 149.84, 147.53, 143.74, 141.19, 140.72, 137.79, 136.77, 136.44, 135.83, 134.58, 131.46, 129.57, 129.44, 128.61, 126.68, 125.99, 125.87, 124.95, 123.65, 122.36, 120.99, 120.69, 120.36, 117.59, 112.34, 111.89, 41.51. ESI-MS (*m/z*) calcd. for C$_{29}$H$_{19}$ClN$_6$O$_3$: 534.96, Found: 507.26 [M-N$_2$+1]$^+$, 509.25 [M-N$_2$+2 + 1]$^+$, 465.30 [M-N$_2$+2 + 2]$^+$. Purity: UP-LC 98.88 %.

2.1.5.3. (E)-3-(1-((1-(7-chloroquinolin-4-yl)-1H-1,2,3-triazol-4-yl)methyl)-1H-indol-3-yl)-1-(3-nitrophenyl)prop-2-en-1-one (7c). Yellow solid, yield: 71 %, R$_f$ = 0.82 (Methanol: dichloromethane = 5 : 95), mp: 236.1–236.9 °C, IR (neat): ν (cm^{-1}) 3157 (C–H)$_{str.}$ triazole ring, 1657 (C═C)$_{str.}$ chalcone. ^{1}H NMR (700 MHz, DMSO-d_6) (δ, ppm): 9.12 (s, 1H, CQ-H), 8.94 (s, 1H, NC-H_{indole}), 8.75 (s, 1H, Ar–H), 8.59 (d, J = 6.86 Hz,1H, C-$H_{triazole}$), 8.45 (d, J = 7.63 Hz, 1H, Ar–H), 8.40 (s, 1H, Ar–H), 8.26 (s, 1H, Ar–H), 8.16–8.12 (m, 3H, Ar–H), 7.97 (d, J = 8.75Hz, 1H, Ar–H), 7.86–7.82 (m, 3H, Ar–H), 7.76–7.70 (m, 2H, Ar–H), 7.35–7.30 (m, 2H, Ar–H), 5.74 (s, 2H, CH_2). ^{13}C NMR (176 MHz, DMSO-d_6) (δ, ppm): 187.39, 152.83, 149.84, 148.64, 143.80, 140.74, 140.23, 140.09, 137.76, 136.81, 135.84, 134.92, 130.99, 129.46, 128.62, 127.16, 126.69, 126.36, 125.87, 123.65, 122.96, 122.31, 121.19, 120.72, 117.63, 115.67, 113.06, 111.87, 41.61. ESI-MS (*m/z*) calcd. for C$_{29}$H$_{19}$ClN$_6$O$_3$: 534.96, Found: 507.26 [M-N$_2$+1]$^+$, 509.25 [M-N$_2$+2 + 1]$^+$, 510.26 [M-N$_2$+2 + 2]$^+$. Purity: UP-LC 94.99 %.

2.1.5.4. (E)-3-(1-((1-(7-chloroquinolin-4-yl)-1H-1,2,3-triazol-4-yl)methyl)-1H-indol-3-yl)-1-(4-nitrophenyl)prop-2-en-1-one (7d). Orange solid, yield: 67 %, R$_f$ = 0.79 (Methanol: dichloromethane = 5 : 95), mp: 247.5–247.9 °C, IR (neat): ν (cm^{-1}) 3142 (C–H)$_{str.}$ triazole ring, 1641 (C═C)$_{str.}$ chalcone. ^{1}H NMR (700 MHz, DMSO-d_6) (δ, ppm): 9.12 (d, 1H, J = 4.62 Hz, CQ-H), 8.94 (s, 1H, NC-H_{indole}), 8.36 (t, J = 4.55 Hz, 3H, C-$H_{triazole}$, Ar–H), 8.32 (d, J = 8.75 Hz, 2H, CH), 8.26 (s, 1H, Ar–H), 8.15 (d, J = 7.91 Hz, 1H, Ar–H), 8.10 (d, J = 15.14 Hz, 1H, Ar–H), 7.97 (d, J = 9.03 Hz, 1H, Ar–H), 7.83 (t, J = 7.07 Hz, 2H, Ar–H), 7.77-7.75 (m, 1H, Ar–H), 7.66 (d, J = 15.4 Hz, 1H, Ar–H), 7.35 (t, J = 7.35 Hz, 1H, Ar–H), 7.30 (t, J = 7.56 Hz, 1H, Ar–H), 5.75 (s, 2H, CH_2). ^{13}C NMR (176 MHz, DMSO-d_6) (δ, ppm): 188.1743, 152.81, 149.92, 149.84, 143.8, 143.78, 140.73, 140.37, 137.81, 137.07, 135.84, 129.99, 129.45, 128.62, 126.69, 126.26, 125.85, 124.27, 123.68, 122.35, 121.27, 120.70, 117.61, 116.11, 113.08, 111.89, 41.59. ESI-MS (*m/z*) calcd. for C$_{29}$H$_{19}$ClN$_6$O$_3$: 534.95; Found: 535.07 [M+H]$^+$, 536.36 [M + H+1]$^+$. Purity: UP-LC 92.70 %.

2.1.5.5. (E)-1-(2-bromophenyl)-3-(1-((1-(7-chloroquinolin-4-yl)-1H-1,2,3-triazol-4-yl)methyl)-1H-indol-3-yl)prop-2-en-1-one (7e). Orange solid, yield: 54 %, R$_f$ = 0.67 (Methanol: dichloromethane = 5 : 95), mp: 190.3–193.0 °C, IR (neat): ν (cm^{-1}) 3151 (C–H)$_{str.}$ triazole ring, 1562 (C═C)$_{str.}$ chalcone. ^{1}H NMR (700 MHz, DMSO-d_6) (δ, ppm): 9.12 (d, J = 4.62 Hz, 1H, CQ-H), 8.91 (s, 1H, NC-H_{indole}), 8.26 (s, 1H, Ar–H), 8.22 (s, 1H, C-$H_{triazole}$), 7.97 (d, 1H$_{trans\ indole\ side}$, J = 9.1 Hz), 7.95 (m, 1H$_{trans\ keto\ side}$ J = 7.98 Hz), 7.81 (t, J = 4.62 Hz, 2H, Ar–H), 7.75 (d, J = 9.03 Hz, 1H, Ar–H), 7.73 (d, J = 7.93 Hz, 1H, Ar–H), 7.58 (d, J = 16.03 Hz, 1H, Ar–H), 7.51–7.49 (m, 2H, Ar–H), 7.44–7.42 (m, 1H, Ar–H), 7.36 (t, J = 7.56 Hz, 1H, Ar–H), 7.25 (t, J = 7.63 Hz, 1H, Ar–H), 7.03 (s, 1H, Ar–H), 5.69 (s, 2H, CH_2). ^{13}C NMR (176 MHz, DMSO-d_6) (δ, ppm): 194.34, 152.81, 149.83, 143.73, 142.00, 141.54, 140.72, 137.82, 136.73, 135.83, 133.47, 131.71, 129.43, 129.41, 128.61, 128.25, 126.69, 125.99, 125.87, 123.64, 122.40, 121.14, 120.86, 120.69, 119.09, 117.58, 112.39, 111.91, 41.51. ESI-MS (*m/z*) calcd. for C$_{29}$H$_{19}$BrClN$_5$O: 568.86, Found: 542.11 [M-N$_2$+2]$^+$, 543.09 [M-N$_2$+2 + 1]$^+$, 545.15 [M-N$_2$+2 + 2+1]$^+$. Purity: UP-LC 91.90 %.

2.1.5.6. (E)-1-(3-bromophenyl)-3-(1-((1-(7-chloroquinolin-4-yl)-1H-1,2,3-triazol-4-yl)methyl)-1H-indol-3-yl)prop-2-en-1-one (7f). Yellow solid, yield: 69 %, R$_f$ = 0.68 (Methanol: dichloromethane = 5: 95), mp: 221.2–221.9 °C, IR (neat): ν (cm^{-1}) 3144 (C–H)$_{str.}$ triazole ring, 1655 (C═C)$_{str.}$ chalcone. ^{1}H NMR (700 MHz, DMSO-d_6) (δ, ppm): 8.91 (s, 1H, NC-H_{indole}), 8.37 (s, 1H, Ar–H), 8.27 (d, 1H, J =

1.96 Hz, C-$H_{triazole}$), 8.22 (s, 1H, Ar–*H*), 8.14 (d, *J* = 7.84 Hz, Ar–*H*), 8.08 (s, 1H, Ar–*H*), 7.97 (d, 1H, *J* = 9.03 Hz, Ar–*H*), 7.83–7.81 (m, 3H, Ar–*H*), 7.77–7.75 (m, 1H, Ar–*H*), 7.65 (d, *J* = 15.4 Hz, 1H, Ar–*H*), 7.52 (t, *J* = 7.84 Hz, 1H, Ar–*H*), 7.34 (t, *J* = 7.42 Hz, 1H, Ar–*H*), 7.29 (t, *J* = 7.77 Hz, 1H, Ar–*H*), 5.74 (s, 2H, C*H*$_2$). ^{13}C NMR (176 MHz, DMSO-d_6) (δ, ppm): 187.88, 152.81, 149.84, 143.85, 140.94, 140.74, 139.43, 137.69, 136.31, 135.83, 135.56, 131.42, 131.04, 129.45, 128.62, 127.73, 126.66, 126.40, 125.87, 123.55, 122.70, 122.20, 121.15, 120.71, 117.61, 115.98, 113.03, 111.79, 41.59. ESI-MS (*m/z*) calcd. for $C_{29}H_{19}BrClN_5O$: 568.86, Found: 542.10 [M-N_2+2]$^+$, 543.16 [M-N_2+2 + 1]$^+$, 545.05 [M-N_2+2 + 2+1]$^+$. Purity: UP-LC 92.37 %.

2.1.5.7. *(E)-1-(4-bromophenyl)-3-(1-((1-(7-chloroquinolin-4-yl)-1H-1,2,3-triazol-4-yl)methyl)-1H-indol-3-yl)prop-2-en-1-one (7g).* Yellow solid, yield: 62 %, R$_f$ = 0.73 (Methanol: dichloromethane = 5: 95), mp: 228.6–229.1 °C, IR (neat): ν (cm^{-1}) 3136 (C–H)$_{str.}$ triazole ring, 1652 (C=C)$_{str.}$ chalcone. ^{1}H NMR (700 MHz, DMSO-d_6) (δ, ppm): 9.12 (d, 1H, *J* = 4.76 Hz, CQ-*H*), 8.93 (s, 1H, NC-*H*$_{indole}$), 8.33 (s, 1H, Ar–*H*), 8.27 (d, *J* = 1.96 Hz, 1H, C-$H_{triazole}$), 8.13 (d, 1H, *J* = 7.91 Hz, Ar–*H*), 8.06 (t, *J* = 8.19 Hz, 3H, Ar–*H*), 7.99–7.96 (m, 2H, Ar–*H*), 7.82 (t, *J* = 4.48 Hz, 2H, Ar–*H*), 7.76–7.73 (m, 3H, Ar–*H*), 7.66 (s, 1H, Ar–*H*), 7.34 (t, *J* = 7.49 Hz, 1H, Ar–*H*), 7.29–7.25 (m, 1H, Ar–*H*), 5.73 (s, 2H, C*H*$_2$). ^{13}C NMR (176 MHz, DMSO-d_6) (δ, ppm): 188.25, 152.81, 149.84, 143.86, 140.73, 139.21, 137.81, 137.72, 136.37, 135.83, 132.24, 130.42, 129.45, 128.62, 126.96, 126.65, 126.31, 125.86, 125.78, 123.55, 122.18, 121.18, 120.71, 117.63, 117.60, 116.02, 113.02, 111.79, 41.55. ESI-MS (*m/z*) calcd. for $C_{29}H_{19}BrClN_5O$: 568.86, Found: 542.16 [M-N_2+2]$^+$, 543.16 [M-N_2+2 + 1]$^+$, 545.05 [M-N_2+2 + 2+1]$^+$. Purity: UP-LC 91.31 %.

2.1.5.8. *2.1.5.8(E)-1-(2-chlorophenyl)-3-(1-((1-(7-chloroquinolin-4-yl)-1H-1,2,3-triazol-4-yl)methyl)-1H-indol-3-yl)prop-2-en-1-one (7h).* Yellow solid, yield: 80 %, R$_f$ = 0.84 (Methanol: dichloromethane = 5 : 95), mp: 207.2–207.6 °C, IR (neat): ν (cm^{-1}) 3149 (C–H)$_{str.}$ triazole ring, 1650 (C=C)$_{str.}$ chalcone. ^{1}H NMR (700 MHz, DMSO-d_6) (δ, ppm): 9.12 (d, 1H, *J* = 4.96 Hz, CQ-*H*), 8.91 (s, 1H, NC-*H*$_{indole}$), 8.26 (d, *J* = 2.1 Hz, 1H, Ar–*H*), 8.23 (s, 1H, C-$H_{triazole}$), 7.97(d, 1H$_{trans\ indole\ side}$, *J* = 9.03 Hz), 7.95 (m, 1H$_{trans\ keto\ side}$ *J* = 7.98 Hz), 7.80 (d, 2H, *J* = 3.71 Hz, Ar–*H*), 7.76–7.74 (m, 1H, Ar–*H*), 7.61 (d, *J* = 16.03 Hz, 1H, Ar–*H*), 7.56 (d, *J* = 1.26 Hz, 1H, Ar–*H*), 7.53–7.51 (m, 2H, Ar–*H*), 7.48–7.46 (m, 2H, Ar–*H*), 7.33 (t, *J* = 7.56 Hz, 1H, Ar–*H*), 7.25 (t, *J* = 7.42 Hz, 1H, Ar–*H*), 7.04 (s, 1H, Ar–*H*), 5.70 (s, 2H, C*H*$_2$). ^{13}C NMR (176 MHz, DMSO-d_6) (δ, ppm): 193.38, 152.81, 149.83, 143.75, 141.32, 140.72, 139.96, 137.81, 136.74, 135.83, 131.69, 130.41, 130.25, 129.54, 129.44, 128.61, 127.81, 126.68, 126.01, 125.87, 123.64, 122.39, 121.33, 120.86, 120.69, 117.59, 112.39, 111.91, 41.51. ESI-MS (*m/z*) calcd. for $C_{29}H_{19}Cl_2N_5O$: 524.41, Found: 496.21 [M – N_2]$^+$, 498.22 [M-N_2+2]$^+$, 499.24 [M-N_2+2 + 1]$^+$. Purity: UP-LC 96.20 %.

2.1.5.9. *(E)-1-(3-chlorophenyl)-3-(1-((1-(7-chloroquinolin-4-yl)-1H-1,2,3-triazol-4-yl)methyl)-1H-indol-3-yl)prop-2-en-1-one (7i).* Yellow solid, yield: 91.4 %, R$_f$ = 0.82 (Methanol: dichloromethane = 5 : 95), mp: 216.6–218.1 °C, IR (neat): ν (cm^{-1}) 3105 (C–H)$_{str.}$ triazole ring, 1652 (C=C)$_{str.}$ chalcone. ^{1}H NMR (700 MHz, DMSO-d_6) (δ, ppm): 8.37 (s, 1H, Ar–*H*), 8.27 (d, 1H, *J* = 1.75 Hz, C-$H_{triazole}$), 8.15 (d, *J* = 7.84 Hz, 1H, Ar–*H*), 8.10-8.08 (m, 2H, CH, Ar–*H*), 8.01 (s, 1H, Ar–*H*), 7.97 (t, *J* = 9.1 Hz, 1H, Ar–*H*), 7.83-7.81 (m, 3H, Ar–*H*), 7.77-7.75 (m, 1H, Ar–*H*), 7.70 (d, *J* = 6.16 Hz, 1H, Ar–*H*), 7.67 (s, 1H, Ar–*H*), 7.59-7.58 (m, 2H, Ar–*H*), 7.33 (d, *J* = 7.77 Hz, 1H, Ar–*H*), 7.30 (d, *J* = 7.77 Hz, 1H, Ar–*H*), 5.74 (s, 2H, C*H*$_2$). ^{13}C NMR (176 MHz, DMSO-d_6) (δ, ppm): 187.94, 152.82, 149.84, 143.85, 140.74, 139.45, 137.69, 136.35, 135.84, 134.18, 132.67, 131.23, 131.17, 129.46, 128.62, 128.18, 127.36, 126.66, 126.39, 125.87, 123.56, 122.21, 121.18, 120.72, 117.62, 116.00, 113.03, 111.78, 41.58. ESI-MS (*m/z*) calcd. for $C_{29}H_{19}Cl_2N_5O$: 524.41, Found: 496.21 [M – N_2]$^+$, 498.17 [M-N_2+2]$^+$, 499.24 [M-N_2+2 + 1]$^+$. Purity: UP-LC 95.68 %.

2.1.5.10. *(E)-1-(4-chlorophenyl)-3-(1-((1-(7-chloroquinolin-4-yl)-1H-1,2,3-triazol-4-yl)methyl) -1H-indol-3-yl)prop-2-en-1-one (7j).* Yellow solid, yield: 52 %, R$_f$ = 0.76 (Methanol: dichloromethane = 5 : 95), mp: 223.2–223.8 °C, IR (neat): ν (cm^{-1}) 3153 (C–H)$_{str.}$ triazole ring, 1648 (C=C)$_{str.}$ chalcone. ^{1}H NMR (700 MHz, DMSO-d_6) (δ, ppm): 9.12 (d, *J* = 4.9Hz, 1H, CQ-*H*), 8.93 (s, 1H, NC-*H*$_{indole}$), 8.33 (s, 1H, Ar–*H*), 8.27 (d, *J* = 1.82 Hz, 1H, (C-$H_{triazole}$), 8.14 (t, *J* = 8.47 Hz, 3H, Ar–*H*), 8.06 (t, *J* = 3.5 Hz, 1H, Ar–*H*), 7.97 (d, *J* = 9.1 Hz, 1H, Ar–*H*), 7.83–7.81 (m, 2H, Ar–*H*), 7.77–7.75 (m, 1H, Ar–*H*), 7.66 (s, 1H, Ar–*H*), 7.61 (d, *J* = 8.33 Hz, 2H, Ar–*H*), 7.35–7.33 (m, 1H, Ar–*H*), 7.30–7.28 (m, 1H, Ar–*H*), 5.73 (s, 2H, C*H*$_2$). ^{13}C NMR (176 MHz, DMSO-d_6) (δ, ppm): 188.07, 152.83, 149.84, 143.86, 140.74, 139.18, 137.83, 137.73, 137.48, 136.37, 135.87, 135.84, 130.59, 130.28, 129.46, 129.29, 129.25, 128.62, 126.66, 126.31, 125.87, 123.57, 122.18, 121.19, 120.72, 117.65, 117.63, 116.04, 113.02, 111.79, 41.55. ESI-MS (*m/z*) calcd. for $C_{29}H_{19}Cl_2N_5O$: 524.41, Found: 496.21 [M-N_2+1]$^+$, 498.22 [M-N_2+2 + 1]$^+$, 499.21 [M-N_2+2 + 2]$^+$. Purity: UP-LC 96.16 %.

2.1.5.11. *(E)-3-(1-((1-(7-chloroquinolin-4-yl)-1H-1,2,3-triazol-4-yl)methyl)-1H-indol-3-yl)-1-(2,4-dichlorophenyl)prop-2-en-1-one (7k).* Yellow solid, yield: 64 %, R$_f$ = 0.77 (Methanol: dichloromethane = 5 : 95), mp: 181.1–182.4 °C, IR (neat): ν (cm^{-1}) 3153 (C–H)$_{str.}$ triazole ring, 1652 1648 (C=C)$_{str.}$ chalcone. ^{1}H NMR (700 MHz, DMSO-d_6) (δ, ppm): 9.12 (d, 1H, *J* = 7.69 Hz, CQ-*H*), 8.91 (s, 1H, NC-*H*$_{indole}$), 8.25 (t, 2H, *J* = 1.82 Hz, Ar–*H*, (C-$H_{triazole}$), 7.96 (t, 2H, *J* = 6.44 Hz, Ar–*H*), 7.81 (d, 2H, *J* = 5.04 Hz, Ar–*H*), 7.75 (s, 2H, Ar–*H*), 7.63 (d, *J* = 15.96 Hz, 1H, Ar–*H*), 7.56 (s, 2H, Ar–*H*), 7.33 (t, *J* = 7.56 Hz, 1H, Ar–*H*), 7.25 (t, *J* = 7.56 Hz, 1H, Ar–*H*), 7.03 (d, *J* = 16.03 Hz, 1H, Ar–*H*), 5.70 (s, 2H, C*H*$_2$). ^{13}C NMR (176 MHz, DMSO-d_6) (δ, ppm): 192.47, 152.81, 149.84, 143.70, 141.98, 140.72, 138.77, 137.84, 137.01, 135.83, 135.38, 131.54, 130.95, 129.96, 129.44, 128.62, 128.05, 126.69, 125.99, 125.86, 123.68, 122.44, 121.02, 120.96, 120.69, 117.59, 112.46, 111.93, 41.52. ESI-MS (*m/z*) calcd. for $C_{29}H_{18}Cl_3N_5O$: 558.85, Found: 532.19 [M-N_2+2]$^+$, 534.17 [M-N_2+2 + 2]$^+$, 535.18 [M-N_2+2 + 2+1]$^+$. Purity: UP-LC 95.71 %.

2.1.5.12. *(E)-3-(1-((1-(7-chloroquinolin-4-yl)-1H-1,2,3-triazol-4-yl)methyl)-1H-indol-3-yl)-1-(2-methoxyphenyl)prop-2-en-1-one (7l).* Cream solid, yield: 53 %, R$_f$ = 0.80 (Methanol: dichloromethane = 5 : 95), mp: 176.4–176.8 °C, IR (neat): ν (cm^{-1}) 3112 (C–H)$_{str.}$

triazole ring, 1663 (C=C)$_{str.}$ chalcone. ^{1}H NMR (700 MHz, DMSO-d_6) (δ, ppm): 9.96 (s, 1H, CQ-*H*), 9.93 (s, 1H, NC-*H*$_{indole}$), 9.12 (d, $J =$ 4.69 Hz, 1H, Ar–*H*), 8.94 (s, 1H, (C-*H*$_{triazole}$), 8.50 (s, 1H, Ar–*H*), 8.36 (s, 1H, Ar–*H*), 8.27 (d, $J =$ 1.82 Hz, 1H, Ar–*H*), 8.13–8.11 (m, 2H, Ar- *H*), 7.96 (d, $J =$ 9.03 Hz, 1H, Ar–*H*), 7.82 (t, $J =$ 4.55 Hz, 2H, Ar–*H*), 7.77–7.75 (m, 1H, Ar–*H*), 7.65 (d, $J =$ 8.26 Hz, 1H, Ar–*H*), 7.36–7.33 (m, 2H, Ar–*H*), 7.03–7.27 (m, 2H, Ar–*H*), 5.27 (s, 2H, C*H*$_2$), 5.24 (s, 2H, OC*H*$_3$). ^{13}C NMR (176 MHz, DMSO-d_6) (δ, ppm): 185.39, 185.31, 152.82, 149.89, 143.63, 141.29, 140.72, 140.62, 137.40, 137.06, 135.84, 129.46, 128.63, 126.76, 125.83, 125.23, 125.17, 124.21, 124.19, 123.27, 123.16, 121.61, 121.56, 120.71, 118.03, 117.61, 111.88, 111.69, 78.48, 77.31, 41.78. ESI-MS (*m/z*) calcd. for C$_{30}$H$_{22}$ClN$_5$O$_2$: 519.99; Found: 518.95 [M – H]$^-$. Purity: UP-LC 96.20 %.

2.1.5.13. (E)-3-(1-((1-(7-chloroquinolin-4-yl)-1H-1,2,3-triazol-4-yl)methyl)-1H-indol-3-yl)-1-(3-methoxyphenyl)prop-2-en-1-one (7 m). Yellow solid, yield: 76 %, R$_f$ = 0.79 (Methanol: dichloromethane = 5 : 95), mp: 198.4–198.8 °C, IR (neat): ν (cm^{-1}) 3151 (C–H)$_{str.}$ triazole ring, 1642 (C=C)$_{str.}$ chalcone. ^{1}H NMR (700 MHz, DMSO-d_6) (δ, ppm): 9.13 (d, 1H, $J =$ 4.9 Hz, CQ-*H*), 8.93 (s, 1H, NC-*H*$_{indole}$), 8.34 (s, 1H, Ar–*H*), 8.27 (s, 1H, (C-*H*$_{triazole}$), 8.10 (d, $J =$ 7.84 Hz, 1H, C*H*), 8.05 (s, 1H, Ar–H), 7.98 (d, $J =$ 9.03 Hz, 1H, Ar–*H*), 7.83–7.81 (m, 3H, Ar–*H*), 7.77 (d, $J =$ 9.03 Hz, 1H, Ar–*H*), 7.73 (d, $J =$ 7.91 Hz, 1H, Ar–*H*), 7.65 (t, $J =$ 10.92 Hz, 1H, Ar–*H*), 7.54 (t, $J =$ 5.25 Hz, 2H, Ar–*H*), 7.49–7.46 (m, 1H, Ar–*H*), 7.33 (t, 1H, $J =$ 7.28 Hz, Ar–*H*), 7.30 (t, $J =$ 8.47 Hz, 1H, Ar–*H*), 7.21–7.20 (m, 1H, Ar–*H*), 5.73 (s, 2H, C*H*$_2$). ^{13}C NMR (176 MHz, DMSO-d_6) (δ, ppm): 189.02, 159.97, 152.89, 149.84, 143.91, 140.75, 140.39, 138.65, 137.67, 135.94, 135.84, 130.35, 130.33, 129.46, 128.62, 126.65, 126.39, 125.88, 123.48, 122.15, 121.14, 121.05, 120.79, 120.72, 118.89, 117.65, 116.63, 113.21, 112.97, 111.77, 55.78, 41.54. ESI-MS (*m/z*) calcd. for C$_{30}$H$_{22}$ClN$_5$O$_2$: 519.99, Found: 492.23 [M-N$_2$+1]$^+$, 494.24 [M-N$_2$+2 + 1]$^+$, 495.19 [M-N$_2$+2 + 2]$^+$. Purity: UP-LC 92.14 %.

2.1.5.14. (E)-3-(1-((1-(7-chloroquinolin-4-yl)-1H-1,2,3-triazol-4-yl)methyl)-1H-indol-3-yl)-1-(4-methoxyphenyl)prop-2-en-1-one (7n). Yellow solid, yield: 63 %, R$_f$ = 0.90 (Methanol: dichloromethane = 5 : 95), mp: 204.2–204.7 °C, IR (neat): ν (cm^{-1}) 3155 (C–H)$_{str.}$ triazole ring, 1646 (C=C)$_{str.}$ chalcone. ^{1}H NMR (700 MHz, DMSO-d_6) (δ, ppm): 9.12 (d, $J =$ 4.69Hz, CQ-*H*), 8.93 (s, 1H, NC-*H*$_{indole}$), 8.29 (s, 1H, Ar–*H*), 8.27 (d, $J =$ 2.1Hz, 1H, (C-*H*$_{triazole}$), 8.14–8.11 (m, 3H, CH, Ar–*H*), 8.01–7.97 (m, 2H, CH, Ar–*H*), 7.83–7.80 (m, 2H, Ar–*H*), 7.77–7.75 (m, 1H, Ar–*H*), 7.70 (s, 1H, Ar–*H*), 7.33 (t, $J =$ 7.42 Hz, 1H, Ar–*H*), 7.28 (t, $J =$ 7.63 Hz, 1H, Ar–*H*), 7.08 (d, $J =$ 8.82 Hz, 2H, Ar–*H*), 5.73 (s, 2H, C*H*$_2$), 3.86 (s, 3H, OC*H*$_3$). ^{13}C NMR (176 MHz, DMSO-d_6) (δ, ppm): 184.22, 160.56, 152.29, 148.57, 143.11, 140.35, 140.47, 138.63, 137.27, 136.23, 135.35, 130.67, 130.23, 128.74, 128.55, 126.35, 126.19, 125.73, 123.18, 122.13, 121.13, 121.65, 120.19, 118.32, 118.19, 117.64, 116.61, 113.71, 112.47, 110.57, 55.38, 41.64. ESI-MS (*m/z*) calcd. for C$_{30}$H$_{22}$ClN$_5$O$_2$: 519.99, Found: 492.27 [M-N$_2$+1]$^+$, 494.24 [M-N$_2$+2 + 1]$^+$, Purity: UP-LC 94.99 %.

2.1.5.15. (E)-3-(1-((1-(7-chloroquinolin-4-yl)-1H-1,2,3-triazol-4-yl)methyl)-1H-indol-3-yl)-1-(3,4-dimethoxyphenyl)prop-2-en-1-one (7o). Yellow solid, yield: 60 %, R$_f$ = 0.73 (Methanol: dichloromethane = 5 : 95), mp: 169.8–171.5 °C, IR (neat): ν (cm^{-1}) 3106 (C–H)$_{str.}$ triazole ring, 1644 (C=C)$_{str.}$ chalcone. ^{1}H NMR (700 MHz, DMSO-d_6) (δ, ppm): 9.12 (d, $J =$ 4.62Hz, 1H, CQ-*H*), 8.93 (s, 1H, NC-*H*$_{indole}$), 8.30 (s, 1H, Ar–*H*), 8.27 (s, 1H, (C-*H*$_{triazole}$)), 8.10 (d, $J =$ 7.84 Hz, 1H, C*H*), 7.99 (d, $J =$ 9.73 Hz, 2H, Ar–*H*), 7.86 (d, $J =$ 8.47 Hz, 1H, CH), 7.82 (t, $J =$ 5.81 Hz, 2H, Ar–*H*), 7.76 (d, $J =$ 9.03 Hz, 1H, Ar–*H*), 7.69 (d, $J =$ 15.47 Hz, 1H, Ar–*H*), 7.59 (s, 1H, Ar–*H*), 7.33 (t, $J =$ 7.35 Hz, 1H, Ar–*H*), 7.28 (t, $J =$ 7.49 Hz, 1H, Ar–*H*), 7.09 (d, $J =$ 8.4 Hz, 1H, Ar–*H*), 5.73 (s, 2H, C*H*$_2$), 3.86 (s, 3H, OC*H*$_3$), 3.86 (s, 3H, OC*H*$_3$). ^{13}C NMR (176 MHz, DMSO-d_6) (δ, ppm): 187.63, 153.17, 152.82, 149.84, 149.22, 143.96, 140.74, 137.62, 137.52, 135.83, 135.37, 131.68, 129.44, 128.62, 126.62, 126.43, 125.86, 123.38, 123.17, 122.01, 120.99, 120.71, 117.59, 116.55, 113.00, 111.71, 111.31, 111.06, 65.39, 56.19, 41.51. ESI-MS (*m/z*) calcd. for C$_{31}$H$_{24}$ClN$_5$O$_3$: 550.02, Found: 522.28 [M – N$_2$]$^+$, 524 [M-N$_2$+2]$^+$. Purity: UP-LC 95.56 %.

2.1.5.16. (E)-3-(1-((1-(7-chloroquinolin-4-yl)-1H-1,2,3-triazol-4-yl)methyl)-1H-indol-3-yl)-1-(thiophen-2-yl)prop-2-en-1-one (7p). Yellow solid, yield: 52 %, R$_f$ = 0.74 (Methanol: dichloromethane = 5 : 95), mp: 218.6–219.1 °C, IR (neat): ν (cm^{-1}) 3147 (C–H)$_{str.}$ triazole ring, 1631 (C=C)$_{str.}$ chalcone. ^{1}H NMR (700 MHz, DMSO-d_6) (δ, ppm): 9.12 (d, $J =$ 4.69 Hz, 1H, CQ-*H*), 8.93 (s, 1H, NC-*H*$_{indole}$), 8.31 (s, 1H, Ar–*H*), 8.26–8.25 (m, 2H, Ar–H, (C-*H*$_{triazole}$), 8.16 (d, $J =$ 7.84 Hz, 1H, Ar–*H*), 8.01 (d, $J =$ 15.33 Hz, 1H, Ar–*H*), 7.98 (t, $J =$ 6.09 Hz, 2H, Ar–*H*), 7.82 (t, $J =$ 4.13 Hz, 2H, Ar–*H*), 7.76–7.75 (m, 1H, Ar–*H*), 7.61 (s, 1H, Ar–*H*), 7.34 (t, $J =$ 7.35 Hz, 1H, Ar–*H*), 7.30–7.28 (m, 2H, Ar–*H*), 5.73 (s, 2H, C*H*$_2$). ^{13}C NMR (176 MHz, DMSO-d_6) (δ, ppm): 181.86, 152.81, 149.84, 146.63, 143.90, 140.73, 137.76, 137.69, 136.12, 135.83, 134.77, 132.74, 129.45, 129.27, 128.62, 126.64, 126.30, 125.87, 123.50, 122.18, 121.23, 120.71, 117.60, 116.26, 112.82, 111.75, 41.54. ESI-MS (*m/z*) calcd. for C$_{27}$H$_{18}$ClN$_5$OS: 495.98; Found: 496.13 [M+1]$^+$, 498.07 [M+2 + 1]$^+$, 499.38 [M+2 + 2]$^+$. Purity: UP-LC 95.58 %.

2.1.5.17. (E)-1-(3,5-bis(benzyloxy)phenyl)-3-(1-((1-(7-chloroquinolin-4-yl)-1H-1,2,3-triazol-4-yl)methyl)-1H-indol-3-yl)prop-2-en-1-one (7q). Off white solid, yield: 71 %, R$_f$ = 0.81 (Methanol: dichloromethane = 5 : 95), mp: 209.8–210.1 °C, IR (neat): ν (cm^{-1}) 3105 (C–H)$_{str.}$ triazole ring, 1651 (C=C)$_{str.}$ chalcone. ^{1}H NMR (700 MHz, DMSO-d_6) (δ, ppm): 9.11 (d, 1H, $J =$ 4.62 Hz, CQ-*H*), 8.93 (s, 1H, NC-*H*$_{indole}$), 8.35 (s, 1H, Ar–*H*), 8.27 (s, 1H, (C-*H*$_{triazole}$), 8.04 (d, $J =$ 8.89 Hz, 2H, Ar–*H*), 7.97 (d, $J =$ 9.1 Hz, 1H, Ar–*H*), 7.81 (t, $J =$ 3.78 Hz, 2H, Ar–*H*), 7.76–7.74 (m, 1H, Ar–H), 7.57 (d, $J =$ 15.47 Hz, 1H, Ar–*H*), 7.48 (d, $J =$ 7.77 Hz, 4H, Ar–*H*), 7.40 (t, $J =$ 7.56 Hz, 4H, Ar–*H*), 7.29 (s, 3H, Ar–*H*), 7.34 (t, $J =$ 7.28 Hz, 3H, Ar–*H*), 6.95 (s, 1H, Ar–*H*), 5.73 (s, 2H, C*H*$_2$), 5.20 (s, 4H, C*H*$_2$). ^{13}C NMR (176 MHz, DMSO-d_6) (δ, ppm): 188.70, 160.12, 152.80, 149.84, 143.89, 141.03, 140.73, 138.69, 137.62, 137.31, 135.83, 135.77, 129.44, 128.95, 128.62, 128.39, 128.26, 126.64, 126.46, 125.87, 123.46, 122.13, 120.95, 120.71, 117.60, 116.51, 112.97, 111.75, 107.49, 106.40, 70.05, 41.56. ESI-MS (*m/z*) calcd. for C$_{43}$H$_{32}$ClN$_5$O$_3$:702.20; Found:702.32 [M]$^+$, 703.32 [M+1]$^+$, 705.36 [M+2 + 1]$^+$. Purity: UP-LC 94.99 %.

2.1.5.18. (E)-3-(1-((1-(7-chloroquinolin-4-yl)-1H-1,2,3-triazol-4-yl)methyl)-1H-indol-3-yl)-1-o-tolylprop-2-en-1-one (7r). Yellow solid, yield: 40 %, R_f = 0.71 (Methanol: dichloromethane = 5 : 95), mp: 178.4–179.2 °C, IR (neat): ν (cm^{-1}) 3144 (C–H)$_{str.}$ triazole ring, 1646 (C=C)$_{str.}$ chalcone.^{1}H NMR (700 MHz, DMSO-d_6) (δ, ppm): 9.11 (d, 1H, J = 4.62 Hz, CQ-H), 8.91 (s, 1H, NC-H_{indole}), 8.26 (s, 1H, Ar–H), 8.21 (s, 1H, (C-$H_{triazole}$), 7.95 (t, J = 8.47 Hz, 2H, Ar–H), 7.80 (t, J = 3.78 Hz, 2H, Ar–H), 7.75 (d, J = 7.28 Hz, 1H, Ar–H), 7.67 (d, J = 15.89 Hz, 1H, Ar–H), 7.52 (d, J = 7.63 Hz, 1H, Ar–H), 7.40 (t, J = 7.42 Hz, 1H, Ar–H), 7.31 (d, J = 14.21 Hz, 3H, Ar–H), 7.25 (t, J = 7.7 Hz, 1H, Ar–H), 7.13 (d, J = 15.96 Hz, 1H, Ar–H), 5.70 (s, 2H, CH_2). ^{13}C NMR (176 MHz, DMSO-d_6) (δ, ppm): 195.82, 152.81, 149.84, 143.85, 140.72, 140.29, 139.96, 137.74, 136.14, 136.0, 135.83, 131.42, 130.37, 129.43, 128.61, 128.12, 126.64, 126.13, 125.86, 123.51, 122.21, 121.57, 120.85, 120.69, 117.58, 112.46, 111.82, 41.47. ESI-MS (*m/z*) calcd. for $C_{30}H_{22}ClN_5O$: 503.99, Found: 504.14 [M+1]$^+$, 505.16 [M+2]$^+$. Purity: UP-LC 95.56 %.

2.1.5.19. (E)-3-(1-((1-(7-chloroquinolin-4-yl)-1H-1,2,3-triazol-4-yl)methyl)-1H-indol-3-yl)-1-(4-fluorophenyl)prop-2-en-1-one (7s). Yellow solid, yield: 80 %, R_f = 0.69 (Methanol: dichloromethane = 5 : 95), mp: 234.5–234.8 °C, IR (neat): ν (cm^{-1}) 3151 (C–H)$_{str.}$ triazole ring, 1648 (C=C)$_{str.}$ chalcone. ^{1}H NMR (700 MHz, DMSO-d_6) (δ, ppm): 9.12 (t, 1H, J = 4.97 Hz, CQ-H), 8.93 (s, 1H, NC-H_{indole}), 8.32 (s, 1H, Ar–H), 8.28 (d, J = 1.96 Hz, 1H, (C-$H_{triazole}$), 8.23 -8.21 (m, 2H, Ar–H), 8.14 (t, J = 8.12 Hz, 2H, Ar–H), 8.04 (d, J = 15.47 Hz, 1H, Ar–H), 7.98 -7.95 (m, 1H, Ar–H), 7.82 (t, J = 4.83 Hz, 3H, Ar–H), 7.77–7.76 (m, 1H, Ar–H), 7.69 (s, 1H, Ar–H), 7.39–7.34 (m, 3H, Ar–H), 7.30 -7.23 (m, 1H, Ar–H), 5.73 (s, 2H, CH_2). ^{13}C NMR (176 MHz, DMSO-d_6) (δ, ppm): 187.76, 165.87, 152.83, 149.84, 144.03, 143.89, 138.84, 137.71, 136.18, 135.81, 131.59, 129.47, 128.62, 126.31, 125.79, 123.51, 122.13, 121.19, 120.72, 117.63, 116.06, 112.99, 111.67, 55.39, 41.53. ESI-MS (*m/z*) calcd. for $C_{29}H_{19}ClFN_5O$: 507.95, Found: 780.23 [M-N_2+1]$^+$, 482.22 [M-N_2+2 + 1]$^+$,483.22 [M-N_2+2 + 2]$^+$, Purity: UP-LC 95.04 %.

2.1.5.20. 1-((1-(7-chloroquinolin-4-yl)-1H-1,2,3-triazol-4-yl)methyl)-1H-indole-3-carbaldehyde (9). Cream solid, yield: 59 %, R_f = 0.71 (Methanol: dichloromethane = 5 : 95), mp: 209.1–209.9 °C, IR (neat): ν (cm^{-1}) 3112 (C–H)$_{str.}$ triazole ring. ^{1}H NMR (700 MHz, DMSO-d_6) (δ, ppm): 9.96 (s, 1H, C-H_{CHO}), 9.12 (d, 1H, J = 4.69 Hz, CQ-H), 8.94 (s, 1H, Ar–H), 8.49 (s, 1H, NC-H_{indole}), 8.26 (d, 1H, J = 2.03 Hz, (C-$H_{triazole}$), 8.12 (d, J = 7.84 Hz, 1H, Ar–H), 7.96 (d, J = 9.1 Hz, 1H, Ar–H), 7.82 (t, J = 4.48 Hz, 2H, Ar–H), 7.76-7.75 (m, 1H, Ar–H), 7.33 (d, J = 7.35 Hz, 1H, Ar–H), 7.28 (d, J = 7.7 Hz, 1H, Ar–H), 5.79 (s, 2H, CH_2). ^{13}C NMR (176 MHz, DMSO-d_6) (δ, ppm): 185.30, 152.82, 149.84, 143.63, 137.39, 135.84, 129.46, 128.62, 126.76, 125.83, 125.23, 124.18, 123.16, 121.55, 120.69, 118.03, 117.61, 111.88, 41.78. ESI-MS (*m/z*) calcd. for $C_{21}H_{14}ClN_5O$: 387.83, Found: 360.07 [M-N_2+1]$^+$, 362.06 [M-N_2+2 + 1]$^+$. Purity: UP-LC 95.68 %.

2.2. Biology

2.2.1. Plasmodium falciparum culture

P. falciparum CQ^S-3D7 and CQ^R-RKL-9 were cultured in human O$^+$ RBCs supplemented with complete RPMI 1640 (Invitrogen, USA), 0.5 % AlbuMax I (Invitrogen, USA), 25 mM NaHCO$_3$ (Sigma, USA), 25 mM HEPES (SRL Pvt. Ltd.), 10 μgml^{-1} gentamicin (Invitrogen, USA), and 0.1 mM hypoxanthine (Invitrogen, USA) according to the method described previously [39]. The parasite culture was maintained in a mixed gas environment (5 % O$_2$, 5 % CO$_2$, and 90 % N$_2$) at 37 °C. Giemsa staining of thin culture smears was used to frequently monitor parasites. 5 % D-sorbitol was used to synchronize parasites at the ring stage.

2.2.2. Growth inhibition assay

SYBR green I (Invitrogen, Carlsbad, USA), a DNA-specific dye, was used to conduct growth inhibition assays to evaluate the inhibitory effect of CQTrICh-analogs against *P. falciparum* 3D7, as described earlier [40,41]. CQ (standard drug) at its IC$_{50}$ value, *i.e.*, 25 nM, served as a positive control. Out of 20 compounds, **7l** and **7r** were selected for further analysis. Initially, parasites (*P. falciparum* CQ^S-3D7 and CQ^R-RKL-9) at the trophozoite stage with 1 % parasitemia maintained at 2 % hematocrit were incubated with different concentrations of **7l** and **7r** ranging 0.62 μM, 1.25 μM, 2.5 μM, 5 μM, 10 μM, and 20 μM, for one complete intra-erythrocytic cycle. Untreated parasites served as negative control and parasites treated with 25 nM of chloroquine (standard) served as positive control. The percent growth inhibition was determined by recording the fluorescence of SYBR green I at excitation and emmision wavelengths of 485 nm and 530 nm, respectively. The experiment was conducted in triplicate, and data were expressed as mean ± SD. % growth inhibition was calculated as follows: % Inhibition = [1 - % parasitemia (treatment)/% Parasitemia (control)] × 100. Giemsa staining was done to observe the parasite morphologically using a light microscope (Olympus).

2.2.3. Blood stage-specific effect

The blood stage-specific inhibitory effects of **7l** and **7r** on CQ^S-3D7 *P. falciparum* was evaluated, as described previously [36]. Briefly, synchronized ring stage parasites (10–12 h) at 0.8 % parasitemia maintained at 2 % hematocrit were treated with **7l** and **7r** at their IC$_{50}$ concentrations in complete RPMI-1640 medium, and seeded in 96-well flat-bottom microtiter plates. The parasite culture was incubated and monitored for up to 56 h post-treatment at 37 °C. Morphological analysis was done by Giemsa staining of the respective cultures using a light microscope (Olympus).

2.2.4. Hemozoin assay

Hemozoin assay was performed as described previously [42]. Synchronized ring-stage parasites (6 % parasitemia) were treated with different concentrations (1.5, 2.5, 5, and 50 μM) of compounds, **7l** and **7r**. In triplicates, samples were seeded into 96-well

flat-bottom plates. After 30 h, samples were treated with 2.5 % SDS in 0.1 M sodium bicarbonate (pH 8.8), and incubated for 10 min at RT. After centrifugation, the pellet was resuspended in 5 % SDS and 50 mM NaOH. After 30 min of incubation, the monomeric heme was quantified by taking absorbance at 405/750 nm ($A_{405\ nm}$ minus $A_{750\ nm}$).

2.2.5. Hemolytic activity

The hemolytic assay was performed as described previously [43]. Briefly, RBC suspension (10 %, v/v) was washed with PBS (pH 7.4) and re-suspended in PBS. The suspension was incubated with **7l** and **7r** at different concentrations for 1 h at 37 °C. Samples were centrifuged, and the supernatant was taken for recording absorbance at 415 nm. Triton X-100 (1 %, v/v)-treated RBCs served as positive control. The experiment was done in triplicate.

2.2.6. Cytotoxicity assay

The calorimetric MTT assay was used to assess the cytotoxicity of compounds towards HEK293 and HepG2 cells [44,45]. In 96-well plate, 2×10^4 (HEK293) and 10^4 (HepG2) cells were seeded with DMEM and 10 % FBS. In a humidified, 5 % CO_2 incubator, the plate was incubated overnight at 37 °C. Compounds **7l** and **7r** were added at doses ranging from 2.5 to 600 μM (HEK293) and 2–500 μM (HepG2), respectively, with untreated cells serving as a control. After 24 h of incubation at 37 °C, 10 μL of MTT (5 mg/mL in PBS) was added to each well. Following incubation, the formazan crystals were dissolved in DMSO. Absorbance at 570 nm was measured using a microplate reader (Thermo Scientific). The assay was performed in triplicate.

2.2.7. Molecular docking studies

To ascertain the binding affinity of **7l** and **7r** for *Pf*CDPK1, molecular docking was performed by using InstaDock, which is a AutoDock Vina-based software [36]. With a blind search space of 62, 58, and 60, centred at −1.465, −20.489, and −19.967 for the X, Y, and Z axes, respectively, the docking was performed using the default docking parameters generated by InstaDock. Using the "ligand splitter" program of the InstaDock software, the docking output was generated for all feasible conformations of the ligands. The generated output was examined based on the docking score, which established the ligands' affinity for binding to *Pf*CDPK1. Docking poses were visualized by PyMOL and Discovery Studio Visualizer.

2.2.8. Computational calculation of physicochemical properties and carcinogenicity

Physicochemical properties, *viz*, molecular weight, heavy atoms, rotatable bonds (RB), H-bond acceptors (HBA), H-bond donors (HBD), Topological Polar Surface Area (TPSA), Log $P_{o/w}$, gastrointentinal (GI) absorption, Lipinski violations, and Pan-Assay INterference Structures (PAINS) alerts of all hybrids **7a-s** and **9** were calculated using SwissADME, an online available tool to compute physicochemical descriptors as well as to predict ADME parameters, pharmacokinetic properties, druglike nature and medicinal chemistry friendliness of one or multiple small molecules to support drug discovery (http://www.swissadme.ch/) [46], and carcinogenicity was predicted by using CarcinoPred-EL, a carcinogenicity prediction web server, which classifies compounds as Carcinogens and Non-Carcinogens using only their two-dimensional structures (EL/about.html" title = "http://112.126.70.33/toxicity/CarcinoPred-EL/about.html">http://112.126.70.33/toxicity/CarcinoPred-EL/about.html) [47].

2.2.9. Microscale thermophoresis (MST) for interaction analysis

Binding affinities of the compounds, **7l** & **7r**, with the recombinant 6xHis-CDPK1 protein (r*Pf*CDPK1) were evaluated by MST analysis, using the Monolith NT.115 instrument (NanoTemper Technologies, Munich, Germany). MST relies on binding-induced changes in thermophoretic mobility, which depends on several molecular properties, including particle charge, size, conformation, hydration state, and solvation entropy. Thus, under constant buffer conditions, thermophoresis of unbound proteins typically differs from the thermophoresis of proteins bound to their interacting partners. The thermophoretic movement of a fluorescently labelled protein is measured by monitoring the fluorescence distribution. The r*Pf*CDPK1/(**7l** or **7r**) interaction analysis protocol was followed as previously described [48,49]. In brief, 10 μM r*Pf*CDPK1 was prepared in HEPES-NaCl buffer (pH 7.5), supplemented with 0.05 % tween-20 to prevent sample aggregation, labelled with 30 μM Cysteine reactive dye (Monolith Protein Labelling Kit Red-Maleimide 2nd Generation, NanoTemper), and incubated in the dark for 30 min at RT. A column (provided by the supplier) was prepared by washing and equilibrating with the buffer. The labelled r*Pf*CDPK1 along with the buffer was added to the column, followed by collecting elution fractions. The elution fraction with fluorescence counts less than 1000 was taken further for interaction analysis. Increasing concentrations of **7l** and **7r** (4.8 nM - 80 μM and 2.4 nM - 40 μM, respectively) diluted in the buffer supplemented with 0.05 % tween-20 were titrated against the constant concentration of the labelled r*Pf*CDPK1. Samples were pre-mixed and incubated for 10 min at RT in the dark, followed by loading of the samples into the standard treated capillaries (K002 Monolith NT.115). The binding experiments were carried out at RT, at 20 % LED power and 40 % MST power. Data evaluation was performed with the Monolith software (Nano Temper, Munich, Germany)

2.2.10. In vitro kinase assay with rPfCDPK1 and HepG2 lysate

The functional activity of r*Pf*CDPK1 was assessed using the ADP-Glo™ Kinase Assay (Promega Corporation), which is an ATP regeneration-based luciferase reaction system rising from nascent ADP phosphorylation. The resulting luminescence signal is proportional to the amount of ADP generated in a particular kinase reaction. Following previously established methods [50,51], phosphorylation assays were carried out with 100 ng (per reaction) of 6xHis-CDPK1, in assay buffer (100 mM Tris-Cl, pH 7.4; 50 mM $MgCl_2$; 2.5 mM DTT; and, 2.5 mM $MnCl_2$). The enzymatic reaction was performed in the presence and absence of Ca^{2+}-ions. Dephosphorylated casein (10 μg per reaction) from bovine milk served as an exogenous substrate for the enzyme. For conditions necessitating the absence

of Ca^{2+}-ions, 2.5 mM EGTA was added. Kinase reactions were started by adding 1 μM ATP and allowed to run for 1 h at 30 °C. To evaluate if the compounds **7l** and **7r** had any inhibitory effects, *Pf*CDPK1 was pre-incubated in the reaction buffer with 1 and 5 μM of each compound for 20 min at RT before starting the reactions with ATP. Following the completion of the reactions, the ADP-Glo™ Kinase Assay was carried out. The resulting luminescence signal was measured using Lumat[3] LB 9508 Ultra-Sensitive Tube Lumin-ometer (Berthold Technologies, U.S.A.).

A similar assay was performed to assess the functional activity of the mammalian kinome, as described previously [52]. Briefly, HepG2 cells (10^7) were re-suspended in 1 mL of lysis buffer (20 mM Tris, pH 7.7; 0.5 % (v/v) Nonidet P-40; 200 mM NaCl; 50 mM NaF, 0.2 mM sodium orthovanadate; $1 \times$ PIC; and, 0.1 % (v/v) 2-mercaptoethanol) for 1 h at 4 °C, centrifuged at 13,000 rpm for 10 min and supernatant was collected. Kinase activity was assessed in the presence of 1 and 5 μM concentrations of **7l** and **7r**.
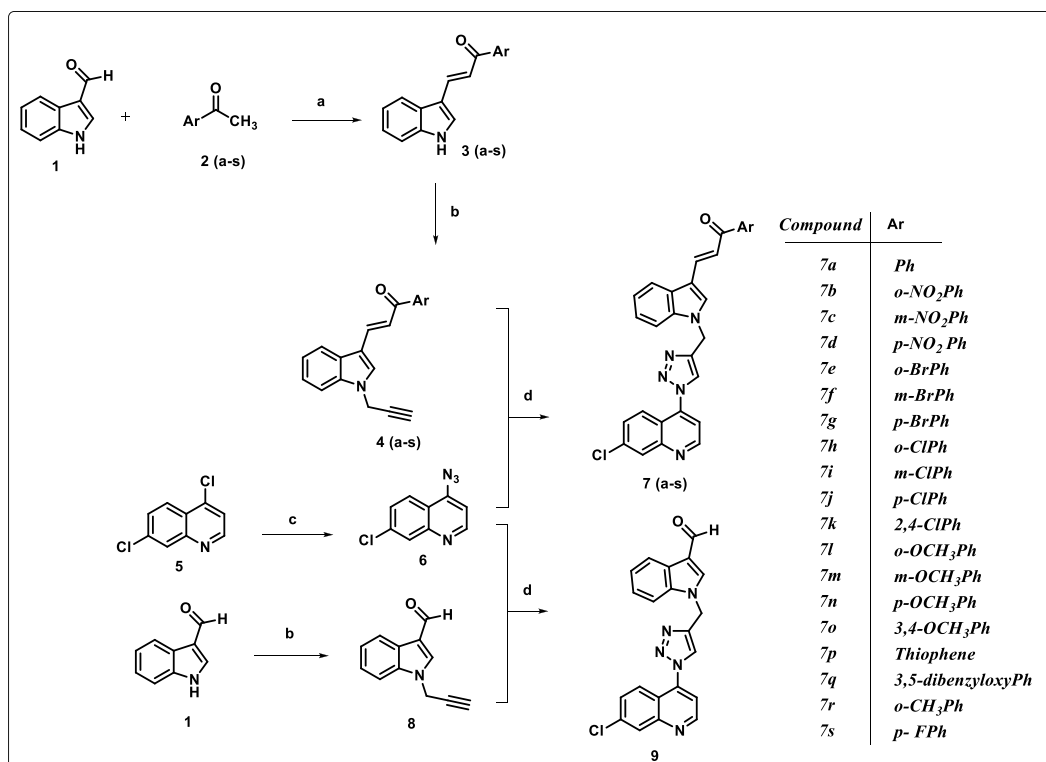
2.2.11. Statistical analysis

The data were subjected to one-way Analysis of Variance (ANOVA) to observe the mean values obtained for control and after treatment with analogs. Dunnett's test was used to compare the treatment and control, and statistical significance was set at $P \leq 0.01$.

3. Results

3.1. Chemistry

Synthesis of CQTrICh-analogs; **7a-s** and **9** were accomplished by an efficient synthetic approach illustrated in Scheme 1. Indole-3-aldehyde (**1**, 1.0 equiv.) on condensation with desired aryl ketones (**2a-s,** 1.0 equiv.) under reflux condition in anhydrous ethanol for 30 h to give indole-chalcones (**3a-s**) in good yield. The indole-chalcone intermediates (**3a-s**) were further propargylated using propargyl bromide (2.0 equiv.) and K_2CO_3 (2.5 equiv.) in DMF at 0 °C then the reaction mixture was allowed to stir at RT for additional 23 h to produce the corresponding alkynes (**4a-s**) in excellent yield. Simultaneously, azide (**6**) [53,54] was prepared from 4,7-dichlor-oquinoline (CQ, **5**) by direct azide replacement using NaN_3 (6.0 equiv.) in anhydrous DMF at 85 °C for 3 h. Then, corresponding alkyne intermediates (**4a-s**) were treated with azide **6** (1 equiv.) at RT for 20–24 h under click reaction [38] in the presence of THF: H_2O (1:2) mixture, sodium ascorbate (0.5 equiv.) and $CuSO_4.5H_2O$ (0.16 equiv.) as a catalyst to afford CQTrICh analogs (**7a-s**) in moderate to good yield (53–91 %). Similarly, we also synthesized compound **9** by treating 1-(prop-2-ynyl)-1H-indole-3-carbaldehyde (**8**) with azide **6** at RT for 20 h under Click reaction in the presence of THF: H_2O (1:2) mixture, sodium ascorbate (0.5 equiv.) and $CuSO_4.5H_2O$ (0.16 equiv.) as a catalyst.

Compound	Ar
7a	*Ph*
7b	*o-NO₂Ph*
7c	*m-NO₂Ph*
7d	*p-NO₂Ph*
7e	*o-BrPh*
7f	*m-BrPh*
7g	*p-BrPh*
7h	*o-ClPh*
7i	*m-ClPh*
7j	*p-ClPh*
7k	*2,4-ClPh*
7l	*o-OCH₃Ph*
7m	*m-OCH₃Ph*
7n	*p-OCH₃Ph*
7o	*3,4-OCH₃Ph*
7p	*Thiophene*
7q	*3,5-dibenzyloxyPh*
7r	*o-CH₃Ph*
7s	*p- FPh*

Scheme 1. Synthesis of CQTrICh analogs (**7a-s**) and **9**. Reagents and conditions: (a) ethanol, reflux, 30 h; (b) propargyl bromide, K_2CO_3, DMF, 0 °C–rt, 23 h; (c) NaN_3, DMF, 85 °C, 3 h; (d) $CuSO_4.5H_2O$, sodium ascorbate, THF/H_2O (1:2), rt, 20–24 h.
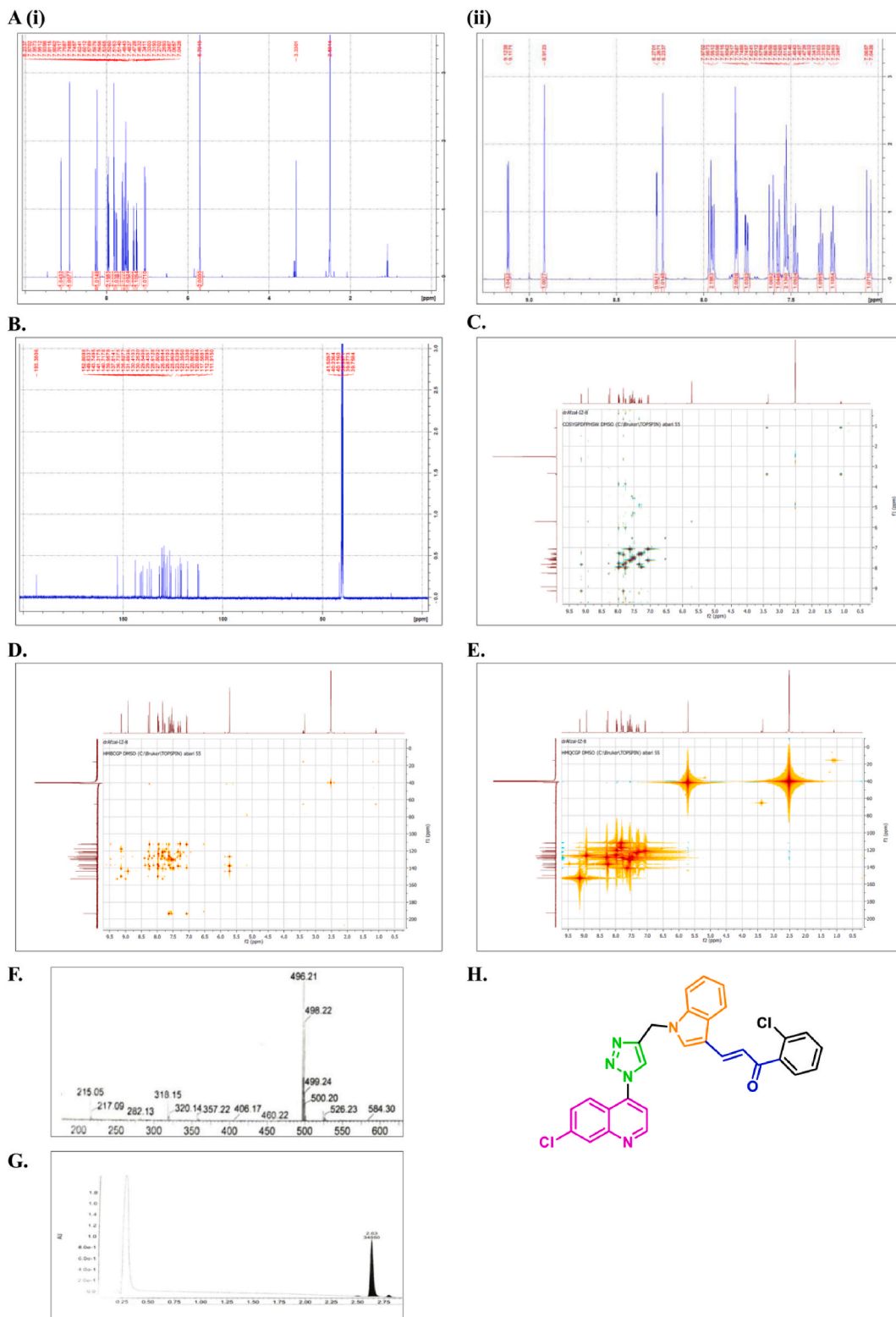
Fig. 2. ^{1}H NMR spectrum (A), ^{13}C NMR spectrum (B), 2D-COSY (C), 2D-HMBC (D), 2D-HMQC (E), mass spectrum (F), purity (G), and structure (H) of (*E*)-1-(2-chlorophenyl)-3-(1-((1-(7-chloroquinolin-4-yl)-1H-1,2,3-triazol-4-yl)methyl)-1H-indol-3-yl)prop-2-en-1-one (7h).
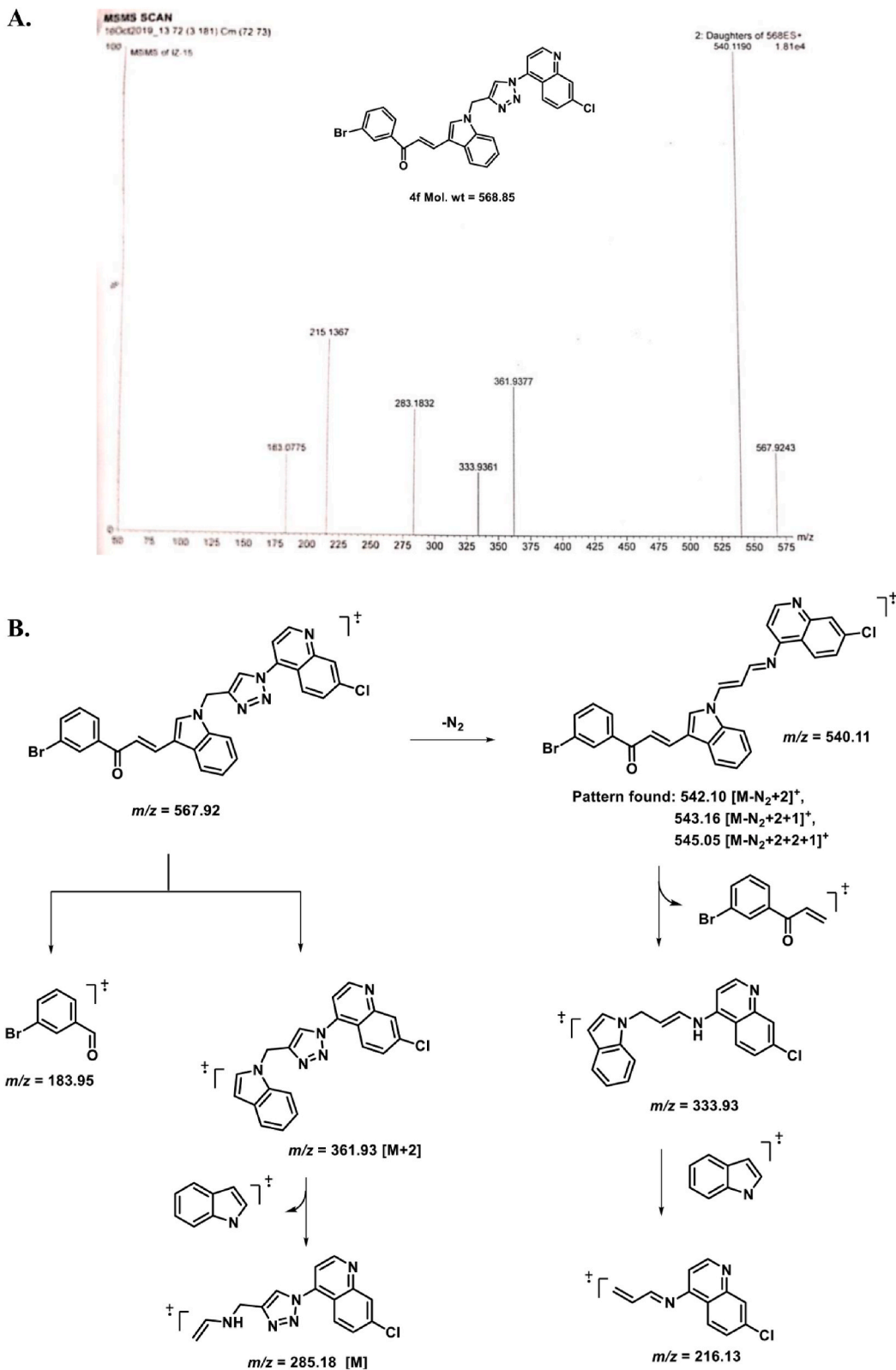
Scheme 2. MS-MS spectrum of **7f (A)** and proposed fragmentation pathway of the protonated ion of the compound **7f (B)**.

All the final CQTrICh analogs (**7a-s**) and **9** were purified by column chromatography using 5 % methanol in dichloromethane as an eluent and obtained an excellent yield followed by characterization and confirmation using spectroscopic techniques such as IR, ^{1}H, ^{13}C NMR, and mass spectrometry. The purity was calculated using UP-LC and obtained with >95 % for most of the analogs whereas few analogs were found with >92 % purity (**Supplementary Figs. S1–S78**).

Among all CQTrICh-analogs (**7a-s**) and **9**, one of the representative compounds (*E*)-1-(2-chlorophenyl)-3-(1-((1-(7-chloroquinolin-4-yl)-1*H*-1,2,3-triazol-4-yl)- methyl)-1*H*-indol-3-yl) prop-2-en-1-one (**7h**) is explained here based on spectroscopic data (Fig. 2); however, similar trend obtained for all other reported analogs of the series. IR spectra of **7h** show a characteristic peak of (C–H)$_{str}$ of triazole ring at 3149 cm^{-1}, whereas a peak at 1650 cm^{-1} confirms the (C=O)$_{str}$ of the chalcone. ^{1}H NMR spectrum of **7h** shows a total of 15 peaks in δ scale (ppm) (Fig. 2A). A doublet appeared at 9.12 indicating the presence of N=C–*H* of the quinoline ring whereas a singlet appeared at 8.91 showing the presence of N=C–*H* of the indole ring and other aromatic peaks (protons of benzene and
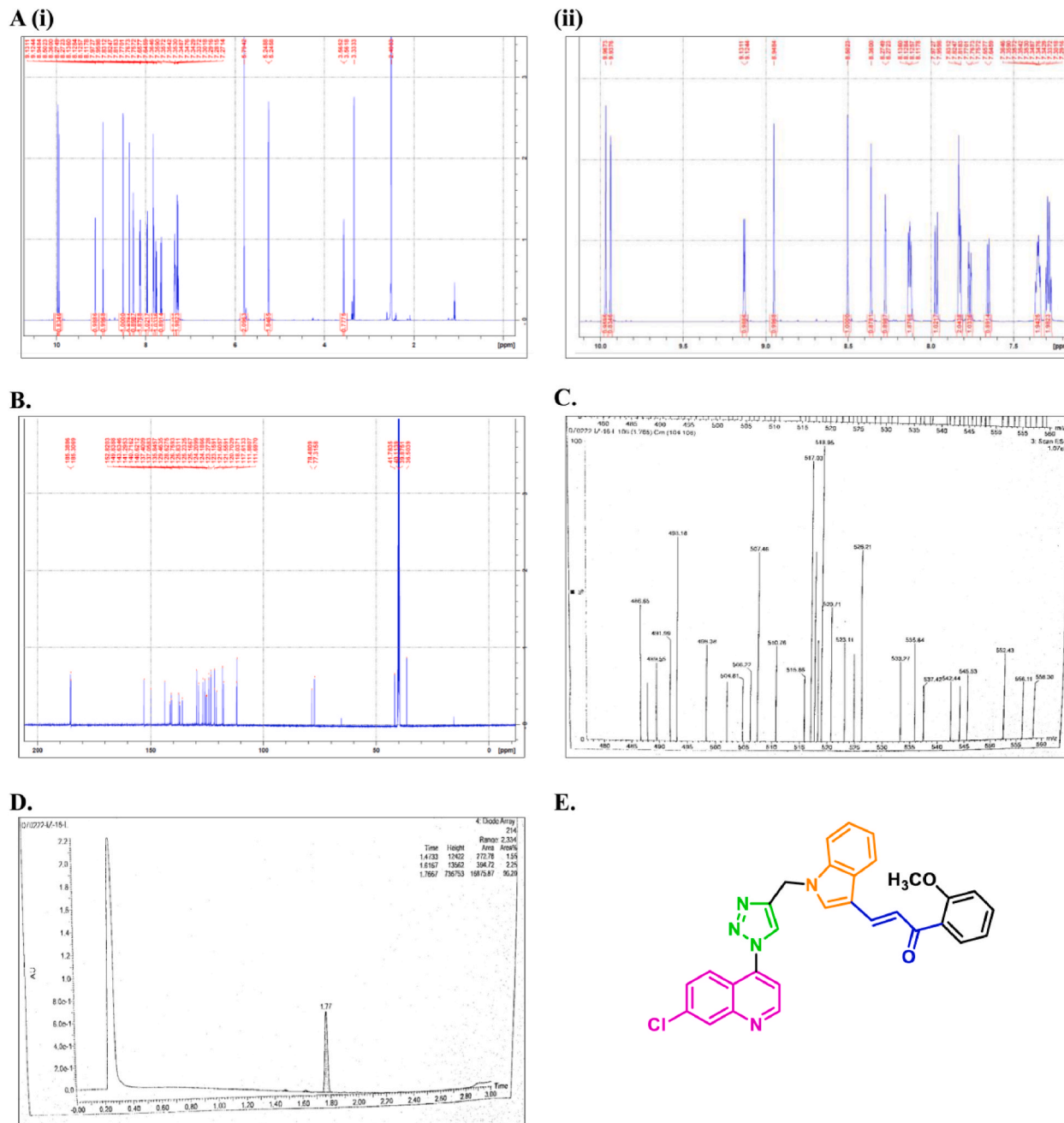
Fig. 3. ^{1}H NMR spectrum (**A**), ^{13}C NMR spectrum (**B**), mass spectrum (**C**), purity (**D**), and structure (**E**) of (E)-3-(1-((1-(7-chloroquinolin-4-yl)-1H-1,2,3-triazol-4-yl)methyl)-1H-indol-3-yl)-1-(2-methoxyphenyl)prop-2-en-1-one (**7l**).

quinoline ring) appear between 8.26-7.04 with their coupling trends. The singlet peak appeared at 8.23 showing the presence of C–*H* of the triazole ring whereas doublet at 7.97 and 7.95 assign the = C-$H_{indole\ side}$ with J = 9.03 Hz and = C-$H_{keto\ side}$ with J = 7.98 Hz in *trans*-conformation of *H*–C=C–*H* group, respectively. The singlet at 5.70, assigns the CH_2 protons present between the indole and triazole ring. ^{13}C NMR spectra (δ, ppm) of **7h** show a total of 29 peaks (Fig. 2B). Some characteristic peaks appeared at 193.38 ppm due to *C*=O, 152.81 (*C*=N$_{quinoline}$), 149.83 (*C*-N$_{quart}$ of quinoline ring), 143.75 (*trans*-C$_{indole\ side}$ = C), 141.32 C$_{quart}$ of benzene, 127.81 (*trans*-C=C$_{ketone\ side}$), 130.41 C$_{quart}$ of triazole ring, 117.59 *C*–H of triazole ring, 112.39 C$_{quart}$ of indole ring carbon, 41.51 CH_2 carbon. These data are well supported by 2D-COSY (Fig. 2C), 2D-HMBC (Fig. 2D), and 2D-HMQC (Fig. 2E) analysis (spectra data not shown). An interesting trend of mass spectrometry also confirms the mass of 7h (Fig. 2F). The mass of 7h was 523.10, whereas in mass spectra we obtained a mass of 496.21 [M-N2]+. As we know, the triazole ring is not that stable on fragmentation patterns, thus, the elimination of N2 (MW = 28) from the triazole ring took place. Therefore, we obtained specific mass patterns of 496.21 [M-N2]+, 498.22 [M-N2+2]+, and 499.24 [M-N2+2 + 1]+ (Fig. 2F). The purity of all the compounds was checked with the UPLC data. In the case of

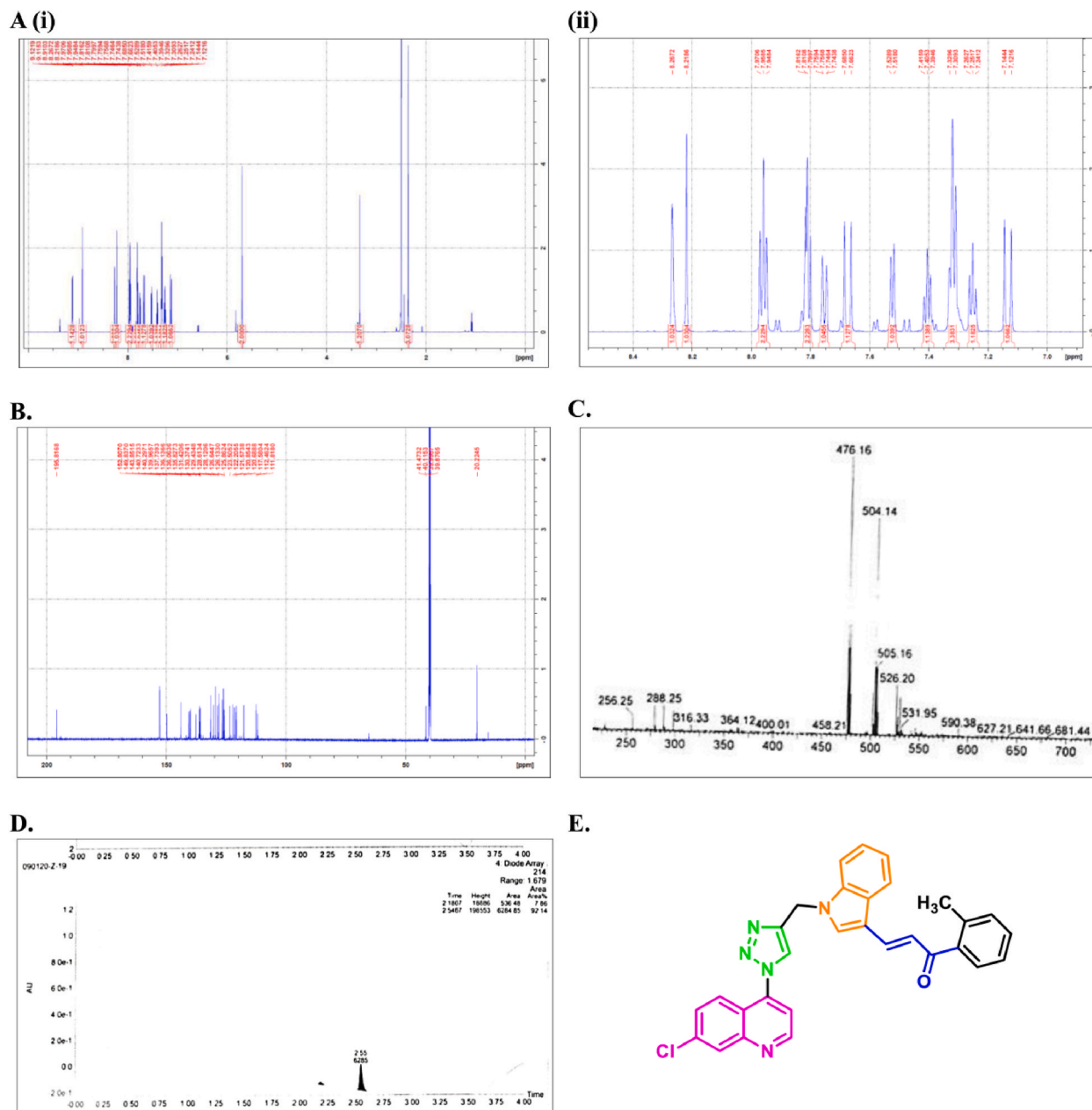**Fig. 4.** ^{1}H NMR spectrum **(A)**, ^{13}C NMR spectrum **(B)**, mass spectrum **(C)**, purity **(D)**, and structure **(E)** of (E)-3-(1-((1-(7-chloroquinolin-4-yl)-1H-1,2,3-triazol-4-yl)methyl)-1H-indol-3-yl)-1-*o*-tolylprop-2-en-1-one **(7r)**.

Table 1

In vitro antimalarial activity of CQTrICh-analogs (**7a-s**) and **9** against the CQ^S-3D7 strain of *P. falciparum*. *% inhibition at 25 nM concentration.

S. no.	Structure	% Inhibition		S. no.	Structure	% Inhibition	
		5 μM	10 μM			5 μM	10 μM
7a		-3.08	36.75	**7k**		4.87	35.33
7b		-5.03	26.13	**7l**		**56.84**	**69.82**
7c		4.82	36.03	**7m**		2.88	48.43
7d		3.86	28.07	**7n**		44.67	55.32
7e		-1.58	47.44	**7o**		-4.00	26.76
7f		47.29	63.51	**7p**		32.14	55.12
7g		12.94	37.38	**7q**		32.14	49.02
7h		42.41	54.25	**7r**		**55.20**	**69.84**
7i		-1.97	33.58	**7s**		15.81	47.15
7j		-0.31	38.62	**9**		-4.99	24.52
CQ		-	52.45*	**CQ**		-	52.45*

7h, the 96.20 % of purity (Fig. 2G) was recorded by UP-LC.

    The characteristic peaks observed within the mass spectra of triazole derivative 7f are shown in Scheme 2(A). These mass spectra exhibit molecular ion peaks and their fragmentation, which confirm the structure of all compounds. A similar trend was found for all compounds. The fragmentation pattern of **7f** as obtained from the mass spectrometry is shown in Scheme 2(B). In a similar manner, the ^{1}H (Figs. 3A and 4A), ^{13}C NMR spectra (Figs. 3B and 4B), mass spectra (Figs. 3C and 4C), purity levels (Figs. 3D and 4D), and structures (Figs. 3E and 4E) of **7l** and **7r** (with potent *in vitro* growth inhibitory activity against *P. falciparum*, as mentioned in section 3.2.1), are shown in Figs. 3 and 4, respectively.

3.2. Biological activity and physicochemical testing

3.2.1. In vitro growth inhibition assay against P. falciparum CQ^S-3D7

    CQTrICh analogs (**7a-s**) and **9** were tested for their *in vitro* antimalarial activity against the CQ^S-3D7 strain of *P. falciparum* at two different concentrations: 5 and 10 μM, and treatment with CQ (standard drug) served as a positive control (Table 1). At a 10 μM concentration, more than 50 % inhibition was achieved for **7f, 7h, 7l, 7n, 7p,** and **7r**, whereas other analogs exhibited >30 % inhibition. However, at a 5 μM concentration, an unexpected trend was observed, and none of the analogs exhibited more than 47 % inhibition, except **7l** and **7r**, which showed 56.84 % and 55.20 % inhibition, respectively. The unexpected trend arises from negative inhibitory concentration due to the formation of precipitates during the screening process. The active CQTrICh analogs **7l** and **7r** exhibited significant percent growth inhibition (>50 %) compared to untreated control against the tested strains of *P. falciparum*. For comparison, we also synthesized compound **9** (without the chalcone unit) to determine whether it is more or less active than the CQTrICh-analogs (**7a-s**). Thus, we observed that compound **9** exhibits poor inhibition among the series at the tested concentration against the CQ^S 3D7 strain of *P. falciparum* confirming the role of chalcone in the antimalarial activity.

    Based on the percent growth inhibition data, both active analogs (**7l** and **7r**) were further screened against *P. falciparum* CQ^S-3D7 and CQ^R-RKL-9 to determine their half-maximal Inhibitory Concentration (IC$_{50}$) values. The IC$_{50}$ of the most effective compounds, **7l** and **7r**, was determined at various concentrations ranging from 0.62 to 20 μM, against *P. falciparum* CQ^S-3D7 and CQ^R-RKL-9, and one complete intra-erythrocytic cycle of *P. falciparum* was examined using SYBR Green I. Both **7l** and **7r** were found to be effective against the tested strains and showed inhibitory effects in a concentration-dependent manner compared to the untreated control. The IC$_{50}$ of compounds **7l** and **7r** were determined to be 2.4 μM and 1.8 μM, respectively, against CQ^S-3D7 strain of *P. falciparum*. Furthermore, **7l** and **7r** were also evaluated against *P. falciparum* CQ^R RKL-9 (Fig. 5A and B, respectively), and IC$_{50}$ values were determined as 3.5 μM and 2.7 μM, respectively, using Graph Pad Prism 8 software. Thus, our results indicate that analogs, **7l** and **7r** are significantly effective
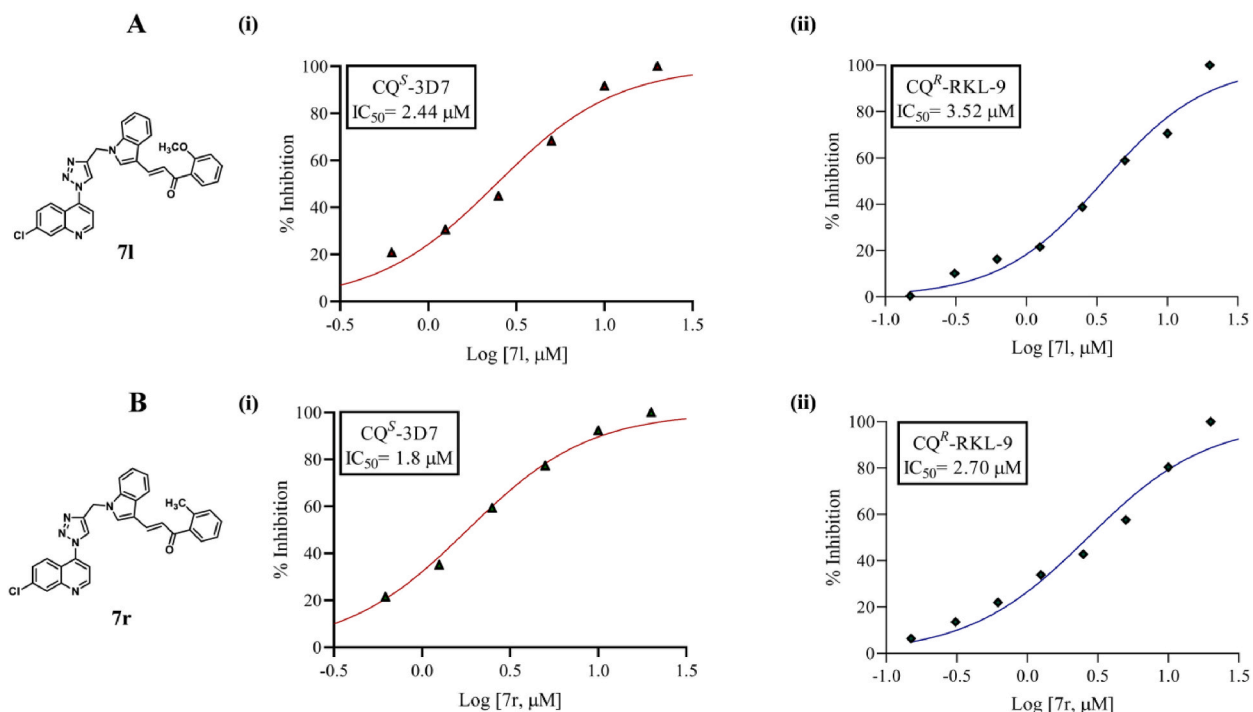
Fig. 5. Growth inhibition assay: Evaluation of IC$_{50}$ values of **7l** and **7r** to check their growth-inhibitory activity against the parasite. Synchronized ring-stage parasites were treated with compounds **7l (A)** and **7r (B)** at concentrations ranging from 0.31 to 20 μM. By plotting growth inhibition values against log concentrations of these compounds, the IC$_{50}$ values of each compound in CQ^S-3D7 **(i)** CQ^R-RKL-9 **(ii)** were determined. The experiment was carried out in triplicate, and the results were expressed as mean values ± SD.

against *P. falciparum* CQ^S-3D7 and CQ^R-RKL-9.

3.2.2. Growth progression analysis

The growth progression evaluation of the potential antimalarial CQTrICh-analogs, **7l** and **7r**, was carried out against the CQ^S-3D7 strain of *P. falciparum* for one complete intra-erythrocytic growth cycle of the parasite. Parasites at ring stage were treated with **7l** and **7r** at their IC$_{50}$ concentrations, and untreated parasites served as control. Thin Giemsa-stained culture smears were prepared at different time intervals of 20, 40, and 56 h post-treatment. The growth progression defect was analyzed by counting ~2000 cells per Giemsa-stained smear by a light microscope (Olympus). Morphological analysis was observed in the presence and absence of the compounds. It was observed that at 40 and 56 h post-treatment, **7l** and **7r** treated parasites were stuck at the trophozoite stage with altered morphology. In the untreated control, the growth of the parasite progressed normally. As compared to the untreated control, a gradual reduction in the percentage of parasitemia was observed (Fig. 6).

3.2.3. Hemozoin inhibition study

During the haemoglobin (Hb) degradation pathway, ferric heme, a by-product of Hb degradation, is toxic to both the malaria parasite and the host cells [55–58]. Consequently, the malaria parasite, for their protection, undergoes a pathway that converts toxic heme into non-toxic metabolites such as crystallization into hemozoin. Hemozoin is a malaria pigment and insoluble in water [59,60]. The free monomeric heme obtained from hemozoin was examined using spectrophotometric analysis. To quantify monomeric heme, synchronized ring-stage parasites were treated with **7l** and **7r** and examined until the schizont stage. The result shows that parasites treated with different concentrations of **7l** and **7r** exhibit a decreased percentage of free monomeric heme in a dose-dependent manner compared to the untreated control. At a 10 μM concentration, **7l** showed 44 %, whereas **7r** showed 48.8 % control-free heme (Fig. 7A). Absorbance was recorded at 405/750 nm which corresponds to the free monomeric heme. The persistence of malaria parasites is dependent on hemozoin crystallization, which has sparked interest in the development of novel antimalarial drugs [31–34].

3.2.4. Hemolysis and cytotoxicity study

The toxicity of compounds, **7l** and **7r**, on human RBCs was observed by evaluating the hemolytic activity at different concentrations ranging from 1.5 to 800 μM. At a maximum concentration of 800 μM, **7l** and **7r** showed marginal toxicity triggering only 4.5 and 5.9 % hemolysis, respectively. However, at a 50 μM concentration, the analogs **7l** and **7r** showed non-toxic nature, resulting in only 1.7 and 2.3 % cell lysis, respectively. Thus, these analogs exhibit no toxicity (Fig. 7B).

The selected compounds were further evaluated for cytotoxicity by the (3-(4,5-dimethyl-2-yl)-2,5-diphenyltetrazolium bromide) (MTT) assay on the noncancerous human cell lines: HEK293, which is an immortalized human embryonic kidney cell line; and HepG2, which is a hepatoblastoma cell line. HEK293 and HepG2 cells are widely used in biological research for decades because of their consistent growth and inclination for transfection. The selected compounds **7l** and **7r** were screened in the concentration range of 2.5–600 μM (HEK293) and 2 − 500 μM (HepG2), and it was found that **7l** and **7r** are non-cytotoxic to the host cells (Fig. 7C and D). It is noteworthy that even at high concentrations of **7l** and **7r**, both hybrids are not cytotoxic to the human cell lines, HEK293 and HepG2,
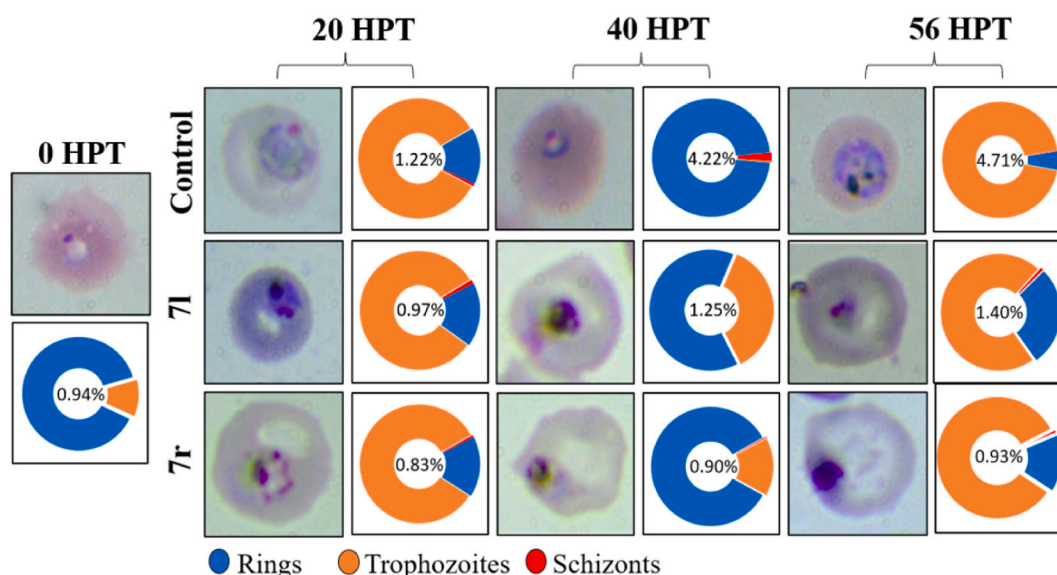
Fig. 6. Light microscopic analysis of intra-erythrocytic stages of *P. falciparum* 3D7, after treatment with the compounds, **7l** and **7r**. Growth progression analysis was conducted for one complete intra-erythrocytic cycle (from ring-to-ring stage), at time intervals of 20, 40, and 56 h post-treatment. Synchronized ring-stage parasite culture of 1 % parasitemia was treated with **7l** and **7r** at their IC$_{50}$ concentrations. Morphological changes were analyzed by Giemsa staining. Graphs and figures show the growth defect during parasite egress or invasion.
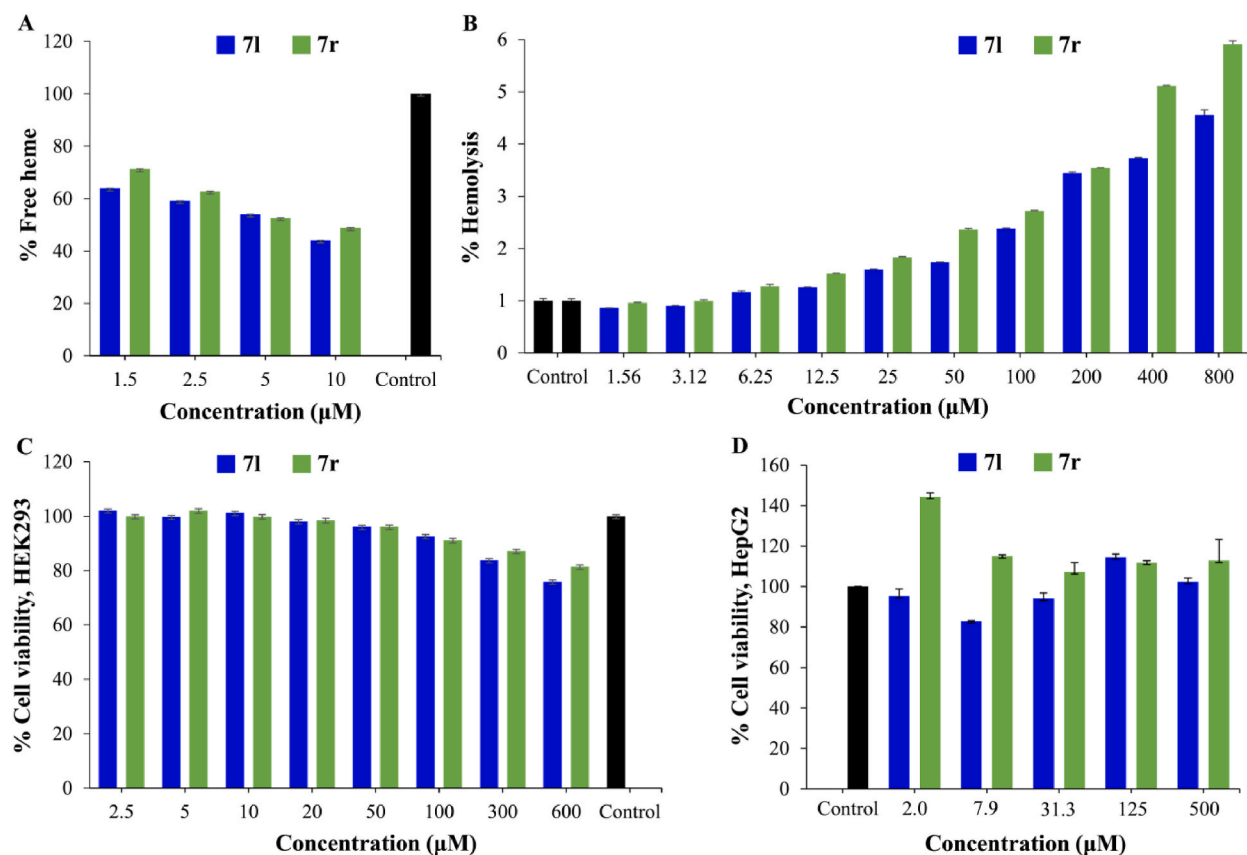
Fig. 7. (A) Graph showing the hemozoin inhibition in parasites exposed to compounds, **7l** and **7r**. Synchronized ring-stage parasites were treated with **7l** and **7r** at different concentrations for 30 h; free heme was calculated by spectrophotometry. **(B)** Effect of triazole hybrids **7l** and **7r** on human RBCs. Hemolytic effect was checked at different concentrations (1.5–800 μM) with 10 % (v/v) RBCs suspension for 1h. Absorbance was recorded at 415 nm indicating no significant lysis even at a higher concentration of **7l** and **7r** (800 μM). MTT assay was done to check the HEK293 **(C)** and HepG2 **(D)** cells' viability after treatment with **7l** and **7r** at various concentrations.

and therefore, determining IC_{50} values, and hence, Selectivity Indices (SI) are not feasible. Based on these results, we can speculate that these compounds might be good anti-malarial entities.

3.2.5. Molecular docking study

In the malaria parasite *P. falciparum*, a targeted gene-disruption approach adopted by Kato et al. demonstrated that *Pf*CDPK1 is essential for the parasite viability by regulating parasite motility during egress and invasion, and performed biochemical screening of a library of 20,000 compounds against purified *Pf*CDPK1 to identify a series of structurally related 2,6,9-trisubstituted purines. SAR studies depicted that quinoline core-containing 2,6,9-trisubstituted purine derivative exhibited potent cellular (EC_{50}: 0.1 μM) and

Table 2
Molecular interaction of **7l** and **7r** with *Pf*CDPK1 and binding affinity of the compounds with *Pf*CDPK1, as deduced from the molecular docking analysis, along with the key interacting residues are depicted.

Target protein	S. no. (Ligand name)	Binding Free Energy (kcal/mol)	pKi	Ligand Efficiency (kcal/mol/non-H atom)	Torsional Energy
*Pf*CDPK1	**7l**	−10.7	7.85	0.2098	2.1791
	7r	−10.2	7.48	0.2082	1.8678

Protein-ligand Interactionsrowhead

S. no.	Affinity (kcal/mol)	Hydrogen Bonds Amino Acid Residues	Distance (Å)	Other Interacting Residues
7l	−10.7	Asp 212	2.67	Val-211, Ile-129, Thr-145, Leu-143, Tyr-148, Phe-213, Phe-147, Lys-85, Leu-120, Phe-147, Glu-146, Ala-83, Leu-198, Leu-62, Gly-151, Val-70, Glu-125, Gly-62, Gly-65, Ala-66,
7r	−10.2	–	–	Thr-125, Lys-85, Asp-212, Val-211, Gly-85, Gly-63, Glu-152, Leu-198, Gly-151, Tyr-148, Phe-147, Leu-62, Glu-195, Ala-83, Glu-146, Val-17, Asn-196, Ile-129

*Pf*CDPK1-inhibitory (IC$_{50}$: 3.846 μM) activities [61]. In the subsequent year, Lemercier et al. studied the structural requirements for the inhibition of *Pf*CDPK1 by developing a primary screening assay, in which a total of 54,000 compounds were tested, yielding two distinct chemical series of small molecules inhibiting *Pf*CDPK1 in nano-molar range, which were further validated through enzymatic and biophysical analysis. One of the active pharmacophores containing an indolizine core (**A**) was shown to inhibit *Pf*CDPK1 with sub-micromolar potency [62]. With this idea, we focused on the indole and quinoline cores to generate CQTrICh-analogs (**7a-s**) and **9**, whereas, quinoline core and chalcones are already known for their potent antimalarial activity [7,8,15,18].

The molecular docking study offers an accurate and preferred orientation of a compound at a receptor molecule's binding site. We conducted the molecular docking studies of **7l** and **7r** to find their possible binding modes with *Pf*CDPK1. We found that **7l** and **7r** preferentially occupied the active site of *Pf*CDPK1 in an energetically stable manner (Table 2 upper panel), with binding energies of −10.7 kcal/mol and −10.2 kcal/mol, respectively. Both the compounds formed several close interactions (such as H-bonds) with the active site residues of *Pf*CDPK1 (Table 2 lower panel). Interaction analysis of all possible docked conformers of the compounds was carried out to investigate their binding pattern and possible interactions with the ATP binding pocket of *Pf*CDPK1 (Fig. 8). Analysis of the docked conformations revealed that **7l** and **7r** bind deeper into *Pf*CDPK1's binding pocket, thereby blocking substrate accessibility, and may be responsible for parasite growth inhibition.

3.2.6. Drug-likeliness assessment

We evaluated the druggability of triazoles by calculating Lipinski's Ro'5 (Rule of five) descriptors. Out of **20** compounds, only **7a, 7p,** and **9** fulfilled all the Ro'5 norms. The computationally calculated physicochemical properties (*viz*, molecular weight, heavy atoms, rotatable bonds (RB), H-bond acceptors (HBA), H-bond donors (HBD), Topological Polar Surface Area (TPSA), Log P$_{o/w}$, gastrointentinal (GI) absorption, Lipinski violations, and PAINS alerts) of all hybrids **7a-s** and **9** are illustrated in Table 3. All triazoles under the study were found to contain less than 15 rotatable bonds. Enones may acts as PAINS and, therefore, may give false positive results in high-throughput screens by reacting non-specifically with numerous biological targets rather than specifically affecting one desired target [63]. However, to address this concern, we computationally predicted the possibility of CQTrICh-analogs (containing
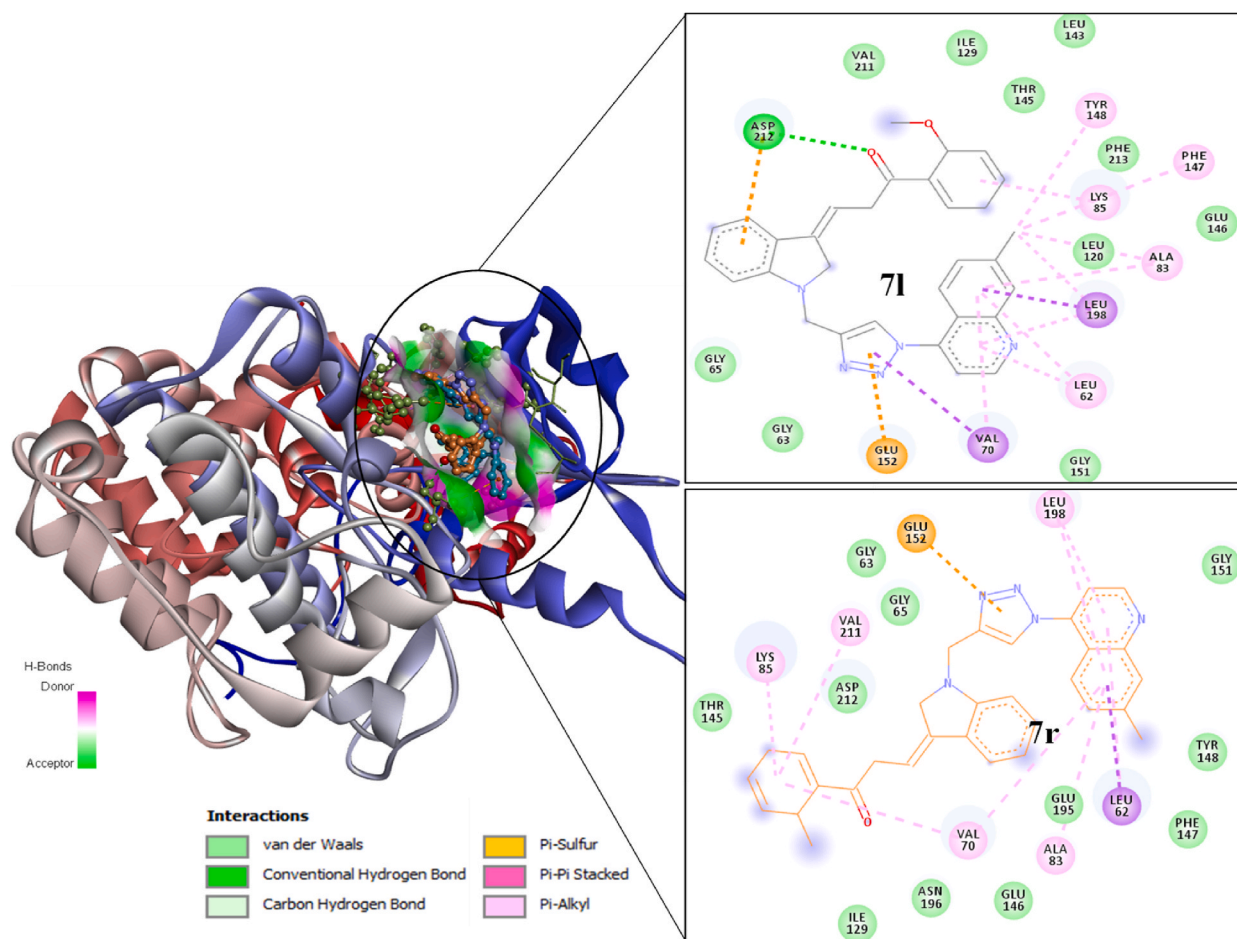

Fig. 8. *In silico* interaction studies of the lead compounds, **7l** and **7r**, and *Pf*CDPK1. Cartoon representation showing that **7l** and **7r** interact within the *Pf*CDPK1 binding pocket (left). 2D images showing hydrogen-bond and hydrophobic interactions of **7l** (upper right) and **7r** (lower right).

Table 3

Computationally calculated physicochemical properties and carcinogenicity of 7a-s and 9 compounds.

Compound ID	cMol. Wt.	cHeavy atoms	cRB	cHBA	cHBD	cTPSA	cLog P	cGI absorption	cLipinski violations	cPAINS alerts	cCarcinogen
7a	489.96	36	6	4	0	65.6	3.91	High	0	0	NC
7b	534.95	39	7	6	0	111.42	3.58	Low	1	0	NC
7c	534.95	39	7	6	0	111.42	3.52	Low	1	0	NC
7d	534.95	39	7	6	0	111.42	3.57	Low	1	0	NC
7e	568.85	37	6	4	0	65.6	4.29	Low	2	0	NC
7f	568.85	37	6	4	0	65.6	4.37	Low	2	0	NC
7g	568.85	37	6	4	0	65.6	4.5	Low	2	0	NC
7h	524.4	37	6	4	0	65.6	4.2	Low	2	0	NC
7i	524.4	37	6	4	0	65.6	4.36	Low	2	0	NC
7j	524.4	37	6	4	0	65.6	4.28	Low	2	0	NC
7k	558.85	38	6	4	0	65.6	4.45	Low	2	0	NC
7l	519.98	38	7	5	0	74.83	4.29	High	1	0	NC
7 m	519.98	38	7	5	0	74.83	4.42	High	1	0	NC
7n	519.98	38	7	5	0	74.83	4.45	High	1	0	NC
7o	550.01	40	8	6	0	84.06	4.25	High	1	0	NC
7p	495.98	35	6	4	0	93.84	4.07	Low	0	0	NC
7q	702.2	52	12	6	0	84.06	5.8	Low	2	0	NC
7r	503.98	37	6	4	0	65.6	4.15	High	2	0	NC
7s	507.95	37	6	5	0	65.6	4.14	Low	2	0	NC
9	387.82	28	4	4	0	65.6	3.01	High	0	0	NC

Physicochemical properties (molecular weight, heavy atoms, rotatable bonds (RB), H-bond acceptors (HBA), H-bond donors (HBD), Topological Polar Surface Area (TPSA), Log $P_{o/w}$, gastrointentinal (GI) absorption, Lipinski violations, and PAINS alerts) of all hybrids **7a-s** and **9** were computationally calculated from SwissADME (http://www.swissadme.ch/) [46], and carcinogenicity was predicted by using CarcinoPred-EL (http://112.126.70.33/toxicity/CarcinoPred-EL/about.html) [47] (c: calculated using SwissADME and CarcinoPred-EL).
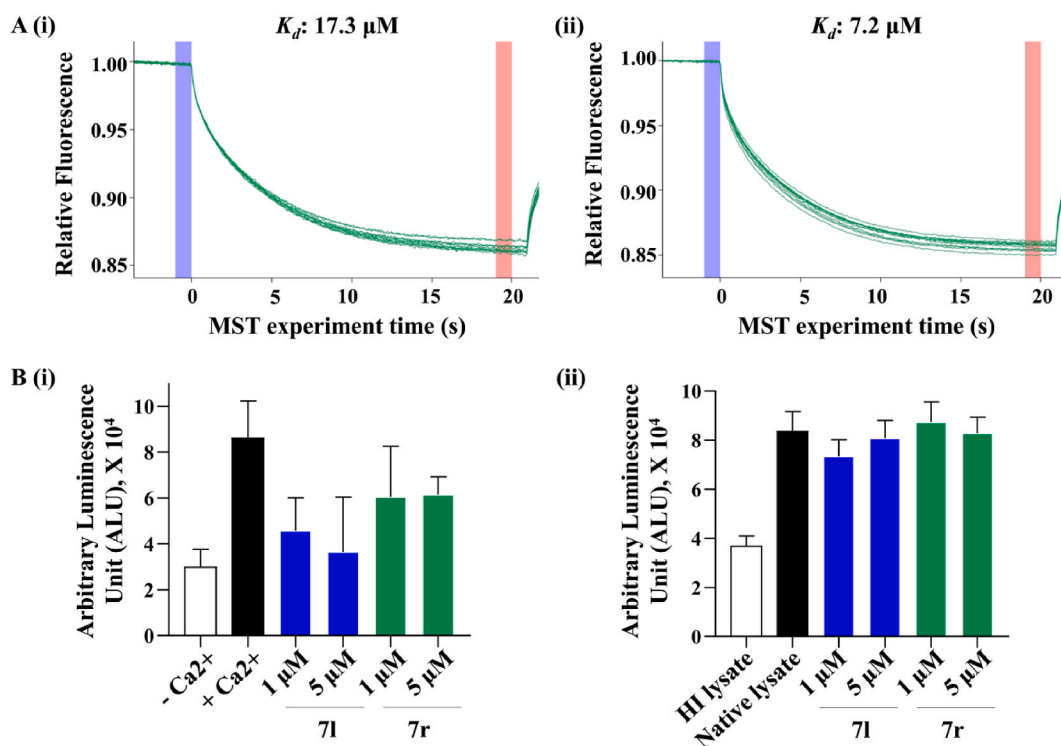
Fig. 9. 7l and 7r interact with and inhibit *Pf*CDPK1-activity *in vitro*. MST was conducted to assess the r*Pf*CDPK/(**7l** or **7r**) interaction *in vitro* **(A)**. Thermophoretic mobility of fluorescently labelled r*Pf*CDPK1 altered dramatically, showing that **7l** and **7r** had an effective interaction, with K_d values of 17.3 μM and 7.2 μM, respectively. Further, *in vitro* kinase assay in the presence of **7l** and **7r** depicted that both compounds showed differential inhibition of *Pf*CDPK1 activity which aligns with our *in silico* docking approach and MST-based interaction analysis **(B(i))**. **7l** and **7r** inhibited phosphorylation activity of *Pf*CDPK1, accounting for 71.9 % and 45.5 % (at 1 μM) and 88.3 % and 43.8 % inhibition (at 5 μM), respectively. **7l** and **7r** were assessed for their effect on host kinase activity inhibition and showed no inhibitory effect on the human kinome **(B(ii))**.

enone moiety) synthesized in this study to act as PAINS. Interestingly, not even a single compound passed the calculated PAIN (cPAIN) alert (Table 3). Additionally, we found that all hybrids are non-carcinogenic in nature.

3.2.7. Compounds interact with and inhibit PfCDPK1 activity in vitro

MST, a novel method for immobilization-free interaction analysis, was used to assess the r*Pf*CDPK1/(**7l** and **7r**) interaction *in vitro*. When fluorescently labelled r*Pf*CDPK1 was titrated against increasing concentrations of **7l** and **7r**, its thermophoretic mobility markedly changed, indicating effective interaction with the compounds. Calculation of equilibrium dissociation constants of **7l** and **7r** revealed K_d *values* of 17.3 μM and 7.2 μM, respectively (Fig. 9A(i) and 9A(ii)). According to Ozbabacan et al., K_d values in this micromolar range are commonly found for transient interactions [64]. Since our *in silico* interaction analysis depicted that the compounds interact with the ATP-binding pocket of *Pf*CDPK1, we used *in vitro* kinase assay to evaluate *Pf*CDPK1 enzymatic activity in the presence of the compounds: **7l** and **7r**, by measuring the amount of ADP generated in the kinase reactions. Both the analogs exhibited differential inhibition of r*Pf*CDPK1 activity which aligns with our *in silico* docking approach and MST-based interaction analysis. Notably, **7l** and **7r** significantly inhibited the phosphorylation activity of r*Pf*CDPK1, accounting for 71.9 % and 45.5 % (at 1 μM) and 88.3 % and 43.8 % inhibition (at 5 μM), respectively (Fig. 9B(i)). We further analyzed the effect of these compounds on mammalian kinome by taking HepG2 cytosolic fraction as kinome source; interestingly, both compounds **7l** and **7r** showed no inhibition of the host kinase activity (Fig. 9B(ii)). Overall, these results suggest that analogs **7l** and **7r** might be active candidates to inhibit the *Pf*CDPK1 enzymatic activity, without affecting the host kinome.
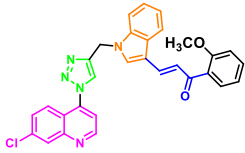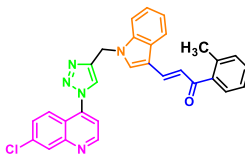
4. Discussion

4-aminoquinoline-based antimalarials containing basic amino group side chains are thought to play a key role in pH trapping and enhance antimalarial activity [27,65]. In indolizines, indole rings which also contain a basic amino group, are well-explored for inhibiting *Pf*CDPK1 with sub-micromolar potency [7]. On the other hand, chalcone-containing side chains in 4-aminoquinoline are also known for their antimalarial activity [7,8]. Thus, with these ideas of antimalarial activity and indole ring involvement in inhibiting *Pf*CDPK1, we have designed and developed CQTrICh-analogs (**7a-s** and **9**) and calculated their Log P-values (cLog P) which were found to lie in a range of 3.52–4.50, whereas compounds **7q** and **9** were reported with cLog P values of 5.80 and 3.01, respectively.

The most active CQTrICh-analogs (**7l** and **7r**) against the CQ^S-3D7 strain were selected and further screened for their *in vitro* antimalarial IC$_{50}$ values against *P. falciparum* CQ^S-3D7 and CQ^R-RKL-9. The selected CQTrICh-analogs (**7l** and **7r**) exhibited IC$_{50}$ values of 2.4 μM, 3.5 μM, and 1.8 μM, 2.7 μM, respectively, against *P. falciparum* CQ^S-3D7 and CQ^R-RKL-9, whereas the Resistance Index (RI) value were determined to be 1.45 (**7l**) and 1.49 (**7r**) (Table 4). The RI value was found to increase with decreasing clog P value in both compounds. An almost linear dependence of RI on clog P suggests that the lack of possible cross-resistance in the tested analogs may be related to their physiochemical properties rather than CQ chemosensitizing itself.

Growth progression analysis was also performed for the active CQTrICh-analogs (**7l** and **7r**) against the CQ^S-3D7 strain of *P. falciparum*, where the parasites at the ring stage were treated with **7l** and **7r**, at their respective IC$_{50}$ concentrations. It was observed that at 40 and 56 h post-treatment, **7l** and **7r**-treated parasites were stuck at trophozoite stage with altered morphology, whereas in the

Table 4
In vitro IC$_{50}$ (μM) of selected potential CQTrICh-analogs (**7l** and **7r**) with their RIs, cLog P-values and *Pf*CDPK1 inhibition activity.

S. no.	Structure	IC$_{50}$ (μM)		RI[a]	cLog P	Cytotoxicity (HEK293)[b]	PI of *Pf*CDPK1[c]	
		CQ^S 3D7	CQ^R RKL-9				1 μM (con.)	5 μM (con.)
7l		2.44	3.52	1.45	4.29	>90 %	71.9 %	88.3 %
7r		1.80	2.70	1.49	4.15	>90 %	45.5 %	43.8 %

dc: calculated using SwissADME (http://www.swissadme.ch/) [46].

[a] Resistance Index (RI)=IC$_{50}$ (μM) CQ^R-RKL-9/CQ^S-3D7.

[b] At 100 μM concentration more than 90 % cell are viable, so can be speculated they are non-toxic to tested non-cancerous human cell lines.

[c] **7l** and **7r** significantly inhibited phosphorylation (PI) activity of *Pf*CDPK1, accounting for 71.9 % and 45.5 % (at 1 μM) and 88.3 % and 43.8 % inhibition (at 5 μM), respectively.

untreated control, the growth of the parasite progressed normally. Overall, in treated cells, a gradual reduction in parasitemia was observed compared to untreated control. Further, at 10 μM concentration, **7l** and **7r**-treated parasites exhibited 44 % and 48.8 % free monomeric heme, respectively, as measured spectrophotometrically. These CQTrICh-analogs (**7l** and **7r**) were also studied for their toxicity on human RBCs at various concentrations ranging from 1.56 to 800 μM. Interestingly, **7l** and **7r** triggered only 4.5 % and 5.9 % hemolysis at a maximum concentration of 800 μM; however, at a 50 μM concentration, **7l** and **7r** showed non-toxic behaviour, resulting in only 1.7 % and 2.3 % cell lysis, respectively. This indicates that the two CQTrICh-analogs are safer to be taken further for pharmacological investigations. Further, CQTrICh-analogs (**7l** and **7r**) were also evaluated for cytotoxicity at various concentrations on noncancerous human cell lines: HEK293 and HepG2. Both tested compounds significantly exhibited >90 % cell viability even at 100 μM concentration. Thus, we can speculate that these analogs are nontoxic and may be potential antimalarial scaffolds.

Overall, if we look at the analogs **7h**, **7l**, and **7r**, an increased inhibitory activity (dose-dependent) was observed when, -Cl (**7h**), -OMe (**7l**), and -Me (**7r**) were located at *ortho*-position in benzene attached to the chalcone unit, which might create a special geometry aiding its interaction with *Pf*CDPK1. These groups might play a major role in enhancing the antimalarial activity, which were validated by hemozoin inhibition, hemolysis, and docking study followed by interaction with *Pf*CDPK1. These speculations were also well-supported by the MST-based interaction analysis of *Pf*CDPK1 and CQTrICh-analogs (**7l** and **7r**), where the equilibrium dissociation constant revealed K_d values of 17.3 μM and 7.2 μM for **7l** and **7r**, respectively. In our *in silico* interaction study, we found that these CQTrICh-analogs (**7l** and **7r**) possibly interact with the ATP binding pocket of *Pf*CDPK1, with binding free energies of −10.7 and −10.2 kcal/mol, and pK_i values of 7.85 and 7.48, respectively. Simultaneously, for **7l** and **7r**, 0.2098 and 0.2082 kcal/mol/non-h atom ligand efficiency were observed along with torsional energy of 2.1791 and 1.8678, respectively. Analog **7l** also exhibited possible protein-ligand interaction with an affinity of −10.7 kcal/mol and formed H-bond with Asp 212 residue of *Pf*CDPK1, whereas **7r** exhibited possible protein-ligand interaction with an affinity of −10.2 kcal/mol, along with other interacting residues (Table 2).

Our Microscale Thermophoresis (MST)-based binding experiments revealed that the lead compounds, **7l** and **7r** interact with r*Pf*CDPK1, exhibiting K_d values of 17.3 and 7.2 μM, respectively (Fig. 9A). These values are crucial when considering the competition with the substrate, *i.e.*, ATP which usually reaches high concentrations within cells, in the range of 1–10 mmol/L, indicating that the compounds may not exert a significant inhibitory effect. However, we want to emphasize that earlier attempts have been made to utilize the scaffolds: indole, triazole, and quinoline, to synthesize novel *specific* inhibitors with their inhibitory activities in the μM range against numerous kinases. In this direction, Xu et al. synthesized a novel [1,2,4]triazolo [4,3-*b*] [1,2,4,5]tetrazine derivative, which was found to be a potent anti-proliferative agent and inhibited c-Met kinase activity (IC$_{50}$: 11.77 μM) [66]. El-Sherief et al. synthesized new 1,2,4-triazole scaffolds, and the majority of the compounds examined had significant anti-proliferative activities against a panel of cancer cell lines [67]. The lead compounds substantially inhibited EGFR and BRAF^{V600E} kinases in the low μM range. In the subsequent year, Goma'a et al. developed and synthesized various 1,2,4-triazole derivatives using ethyl 2-((5-amino-1H-1,2, 4-triazol-3-yl)thio)acetate as the starting material [68]. At an 80 μM dosage, the lead compound reduced viral plaques by 50 % against Herpes Simplex Virus-1 (HSV-1) grown on Vero African green monkey kidney cells. According to docking studies, the lead compound interacted with the active site of HSV-1 thymidine kinase.

In the malaria parasite *P. falciparum*, a targeted gene-disruption approach adopted by Nobutaka Kato et al. (2008) demonstrated that *pfcdpk1* is essential for the parasite viability by regulating parasite motility during egress and invasion, and identified a series of structurally related 2,6,9-trisubstituted purines by an *in vitro* biochemical screening using recombinant *Pf*CDPK1 against a library of 20,000 compounds [61]. SAR studies of the 2,6,9-trisubstituted purines yielded compound **14** harboring a quinoline moiety, which showed potent *Pf*CDPK1-inhibitory (IC$_{50}$: 3.8 μM) activities. Our research group recently used a structure-based virtual chemical library screening approach in conjunction with extensive biochemical and biophysical characterization-based tools to identify novel lead candidates: Compound 1$_{(ST092793)}$ and Compound 2$_{(S344699)}$, both of which can inhibit *Pf*CDPK1 activity *in vitro*. The compounds' IC$_{50}$ values for *Pf*CDPK1-inhibitory activity were 33.8 and 42.6 μM, respectively; while the compounds displayed intra-erythrocytic growth inhibition of the parasite, with IC$_{50}$ values of 9.5 and 17.8 μM, respectively [50].

Based on the *in silico* results, we performed *in vitro* kinase assay to demonstrate the enzymatic activity of *Pf*CDPK1 in the presence of CQTrICh-analogs (**7l** and **7r**) by measuring the ADP formed during the kinase reaction. Both (**7l** and **7r**) significantly inhibited phosphorylation activity of *Pf*CDPK1, accounting for 28.2 % and 54.5 % (at 1 μM), and, 11.6 % and 56.2 % (at 5 μM) inhibition, respectively (Table 4). Analog **9** (without chalcone) was not a good inhibitor in a concentration-dependent analysis. Thus, the overall findings and observations synchronize well with each other.

5. Conclusion

A successful synthesis of a series of CQTrICh-analogs **(7a-s)** and **9** using click chemistry generated **7l** and **7r**, likely to be potential antimalarial analogs. In fact, these analogs proved to be potential and valuable probes of antimalarial activity, resistance, and are nontoxic in nature. The 4-aminoquinoline bearing triazole, indole, and chalcone units were also found to be reasonably eye-opening probe due to their significant contribution to the inhibition of phosphorylation activity of *Pf*CDPK1. These probes or analogs might open a new way of thinking towards designing novel antimalarials.

All the synthesized analogs were screened for their *in vitro* antimalarial activity, and the most active analogs were evaluated further for their IC$_{50}$ values against *P. falciparum* CQ^S-3D7 and CQ^R-RKL-9, where **7l** (*o*-methoxy) and **7r** (*o*-methyl) were found to be effective against the tested strains with IC$_{50}$ values (against *P. falciparum* CQ^S-3D7 and CQ^R-RKL-9) of 2.4, 3.5 μM and 1.8, 2.7 μM, respectively. The RI values were obtained as 1.45 (**7l**) and 1.49 (**7r**). At a 10 μM concentration, **7l** and **7r** exhibited 44 % and 48 % control-free heme, respectively, whereas at a 50 μM concentration, both compounds were found to be non-toxic in nature. Both the selected analogs were also found to be non-cytotoxic to HEK293 and HepG2 cells. Additionally, the docking study revealed that **7l** and **7r** exhibit good

binding affinity for *Pf*CDPK1 and occupy the ATP-binding site. *In vitro* activity also supported the *in silico* docking approach. Analogs, **7l** exhibited better inhibition (28 % at 1 μM, 11.6 % at 5 μM) as compared to **7r** (54.5 % at 1 μM and 56.2 % at 5 μM) against *Pf*CDPK1. Overall, the results indicate that the selected CQTrICh-analogs (**7r** and **7l**) are promising *Pf*CDPK1 inhibitors with antimalarial activity.

This is the first attempt in which we have designed CDPK1 inhibitors by implementing a hybridization approach; however, it still needs further enhancements. The antimalarial properties of chalcones based on indole and different aryl/heteroaryl moieties are well documented in the literature. The idea to conjugate these chalcones with CQ via a triazole linker intended to enhance their efficacy and selectivity against the malaria parasite. Fortunately, we found two analogs that were equipotent against both CQ^S-3D7 and CQ^R-RKL-9 strains of *P. falciparum*, a reasonable start for a new series. We are now intrigued to enhance the efficacy of these analogs by using computational as well as SAR approaches, and optimizing the CQ and side-chain parts. This would require additional planning to design, synthesize, characterize, and perform their detailed biological analysis, including CDPK1 inhibition studies.

Data availability statement

Data associated with our study has not been deposited into a publicly available repository. Data will be made available upon request from the corresponding author.

CRediT authorship contribution statement

Iram Irfan: Writing – original draft, Methodology, Investigation, Formal analysis, Data curation, Conceptualization. **Amad Uddin:** Writing – original draft, Methodology, Investigation, Formal analysis, Data curation, Conceptualization. **Ravi Jain:** Writing – review & editing, Writing – original draft, Methodology, Investigation, Data curation. **Aashima Gupta:** Writing – original draft, Methodology, Investigation, Data curation. **Sonal Gupta:** Writing – original draft, Methodology, Investigation, Data curation. **John V. Napoleon:** Writing – review & editing. **Afzal Hussain:** Formal analysis, Data curation. **Mohamed F. Alajmi:** Formal analysis, Data curation. **Mukesh C. Joshi:** Writing – review & editing, Formal analysis. **Phool Hasan:** Formal analysis. **Purnendu Kumar:** Writing – review & editing. **Mohammad Abid:** Writing – original draft, Supervision, Resources, Project administration, Funding acquisition, Formal analysis, Data curation, Conceptualization. **Shailja Singh:** Writing – original draft, Supervision, Resources, Project administration, Funding acquisition, Formal analysis, Data curation, Conceptualization.

Declaration of competing interest

The authors declare that they have no known competing financial interests or personal relationships that could have appeared to influence the work reported in this paper.

Acknowledgments

Appendix A. Supplementary data

Supplementary data to this article can be found online at https://doi.org/10.1016/j.heliyon.2024.e25077.

References

[1] H. Hussain, S. Specht, S.R. Sarite, A. Hoerauf, K. Krohn, New quinoline-5,8-dione and hydroxynaphthoquinone derivatives inhibit a chloroquine resistant Plasmodium falciparum strain, Eur. J. Med. Chem. 54 (2012), https://doi.org/10.1016/j.ejmech.2012.06.046.

[2] S. Kumar, M. Guha, V. Choubey, P. Maity, U. Bandyopadhyay, Antimalarial drugs inhibiting hemozoin (β-hematin) formation: a mechanistic update, Life Sci. 80 (2007) 813–828, https://doi.org/10.1016/j.lfs.2006.11.008.

[3] K.K. Roy, Targeting the active sites of malarial proteases for antimalarial drug discovery: approaches, progress and challenges, Int. J. Antimicrob. Agents 50 (2017) 287–302, https://doi.org/10.1016/j.ijantimicag.2017.04.006.

[4] B. Li, T.J. Webster, Bacteria antibiotic resistance: new challenges and opportunities for implant-associated orthopedic infections, J. Orthop. Res. 36 (2018) 22–32, https://doi.org/10.1002/jor.23656.

[5] A. Uddin, M. Chawla, I. Irfan, S. Mahajan, S. Singh, M. Abid, Medicinal chemistry updates on quinoline- and endoperoxide-based hybrids with potent antimalarial activity, RSC Med. Chem. 12 (2021), https://doi.org/10.1039/d0md00244e.

[6] WHO, World Malaria Report, World Malaria Report, 2021.

[7] T. Hänscheid, T.J. Egan, M.P. Grobusch, Haemozoin: from melatonin pigment to drug target, diagnostic tool, and immune modulator, Lancet Infect. Dis. 7 (2007), https://doi.org/10.1016/S1473-3099(07)70238-4.

[8] T.J. Egan, Recent advances in understanding the mechanism of hemozoin (malaria pigment) formation, J. Inorg. Biochem. 102 (2008), https://doi.org/10.1016/j.jinorgbio.2007.12.004.

[9] V.K. Zishiri, M.C. Joshi, R. Hunter, K. Chibale, P.J. Smith, R.L. Summers, R.E. Martin, T.J. Egan, Quinoline antimalarials containing a dibemethin group are active against chloroquinone-resistant plasmodium falciparum and inhibit chloroquine transport via the P. falciparum chloroquine-resistance transporter (PfCRT), J. Med. Chem. 54 (2011), https://doi.org/10.1021/jm2009698.

[10] S. Andrews, S.J. Burgess, D. Skaalrud, J.X. Kelly, D.H. Peyton, Reversal agent and linker variants of reversed chloroquines: activities against Plasmodium falciparum, J. Med. Chem. 53 (2010), https://doi.org/10.1021/jm900972u.

[11] S.J. Burgess, A. Selzer, J.X. Kelly, M.J. Smilkstein, M.K. Riscoe, D.H. Peyton, A chloroquine-like molecule designed to reverse resistance in Plasmodium falciparum, J. Med. Chem. 49 (2006), https://doi.org/10.1021/jm060399n.

[12] S.J. Burgess, J.X. Kelly, S. Shomloo, S. Wittlin, R. Brun, K. Liebmann, D.H. Peyton, Synthesis, Structure-activity relationship, and mode-of-action studies of antimalarial reversed chloroquine compounds, J. Med. Chem. 53 (2010), https://doi.org/10.1021/jm1006484.

[13] M.C. Joshi, T.J. Egan, Quinoline containing side-chain antimalarial analogs: Recent advances and therapeutic Application, Curr. Top. Med. Chem. 20 (2020), https://doi.org/10.2174/1568026620666200127141550.

[14] M.C. Joshi, J. Okombo, S. Nsumiwa, J. Ndove, D. Taylor, L. Wiesner, R. Hunter, K. Chibale, T.J. Egan, 4-Aminoquinoline antimalarials containing a Benzylmethylpyridylmethylamine group are active against drug resistant plasmodium falciparum and exhibit oral activity in mice, J. Med. Chem. 60 (2017), https://doi.org/10.1021/acs.jmedchem.7b01537.

[15] E.M. Guantai, K. Ncokazi, T.J. Egan, J. Gut, P.J. Rosenthal, P.J. Smith, K. Chibale, Design, synthesis and in vitro antimalarial evaluation of triazole-linked chalcone and dienone hybrid compounds, Bioorganic Med. Chem. 18 (2010), https://doi.org/10.1016/j.bmc.2010.10.009.

[16] F. Shah, P. Mukherjee, J. Gut, J. Legac, P.J. Rosenthal, B.L. Tekwani, M.A. Avery, Identification of novel malarial cysteine protease inhibitors using structure-based virtual screening of a focused cysteine protease inhibitor library, J. Chem. Inf. Model. 51 (2011) 852–864, https://doi.org/10.1021/ci200029y.

[17] K.V. Sashidhara, M. Kumar, R.K. Modukuri, R.K. Srivastava, A. Soni, K. Srivastava, S.V. Singh, J.K. Saxena, H.M. Gauniyal, S.K. Puri, Antiplasmodial activity of novel keto-enamine chalcone-chloroquine based hybrid pharmacophores, Bioorganic Med. Chem. 20 (2012) 2971–2981, https://doi.org/10.1016/j.bmc.2012.03.011.

[18] R. Kant, D. Kumar, D. Agarwal, R.D. Gupta, R. Tilak, S.K. Awasthi, A. Agarwal, Synthesis of Newer 1,2,3-triazole Linked Chalcone and Flavone Hybrid Compounds and Evaluation of Their Antimicrobial and Cytotoxic Activities, Elsevier Ltd, 2016, https://doi.org/10.1016/j.ejmech.2016.02.041.

[19] N. Devender, S. Gunjan, R. Tripathi, R.P. Tripathi, Synthesis and antiplasmodial activity of novel indoleamide derivatives bearing sulfonamide and triazole pharmacophores, Eur. J. Med. Chem. 131 (2017) 171–184, https://doi.org/10.1016/j.ejmech.2017.03.010.

[20] S. Oramas-Royo, P. López-Rojas, Á. Amesty, D. Gutiérrez, N. Flores, P. Martín-Rodríguez, L. Fernández-Pérez, A. Estévez-Braun, Synthesis and antiplasmodial activity of 1,2,3-triazole-naphthoquinone conjugates, Molecules 24 (2019) 1–23, https://doi.org/10.3390/molecules24213917.

[21] I. Wadi, D. Prasad, N. Batra, K. Srivastava, A.R. Anvikar, N. Valecha, M. Nath, Targeting asexual and Sexual blood stages of the human malaria parasite P. Falciparum with 7-chloroquinoline-based 1,2,3-triazoles, ChemMedChem 14 (2019) 484–493, https://doi.org/10.1002/cmdc.201800728.

[22] S. Kumar, M. Kumar, R. Ekka, J.D. Dvorin, A.S. Paul, A.K. Madugundu, T. Gilberger, H. Gowda, M.T. Duraisingh, T.S. Keshava Prasad, P. Sharma, PfCDPK1 mediated signaling in erythrocytic stages of Plasmodium falciparum, Nat. Commun. 8 (2017) 63, https://doi.org/10.1038/s41467-017-00053-1.

[23] K.H. Ansell, H.M. Jones, D. Whalley, A. Hearn, D.L. Taylor, E.C. Patin, T.M. Chapman, S.A. Osborne, C. Wallace, K. Birchall, J. Large, N. Bouloc, E. Smiljanic-Hurley, B. Clough, R.W. Moon, J.L. Green, A.A. Holder, Biochemical and Antiparasitic properties of inhibitors of the plasmodium falciparum calcium-dependent protein kinase PfCDPK1, Antimicrob. Agents Chemother. 58 (2014) 6032–6043, https://doi.org/10.1128/aac.02959-14.

[24] T.M. Chapman, S.A. Osborne, N. Bouloc, J.M. Large, C. Wallace, K. Birchall, K.H. Ansell, H.M. Jones, D. Taylor, B. Clough, J.L. Green, A.A. Holder, Substituted imidazopyridazines are potent and selective inhibitors of Plasmodium falciparum calcium-dependent protein kinase 1 (PfCDPK1), Bioorganic Med. Chem. Lett. 23 (2013) 3064–3069, https://doi.org/10.1016/j.bmcl.2013.03.017.

[25] T.M. Chapman, S.A. Osborne, C. Wallace, K. Birchall, N. Bouloc, H.M. Jones, K.H. Ansell, D.L. Taylor, B. Clough, J.L. Green, A.A. Holder, Optimization of an imidazopyridazine series of inhibitors of plasmodium falciparum calcium-dependent protein kinase 1 (Pf CDPK1), J. Med. Chem. 57 (2014) 3570–3587, https://doi.org/10.1021/jm500342d.

[26] D.C. Schuck, A.K. Jordão, M. Nakabashi, A.C. Cunha, V.F. Ferreira, C.R.S. Garcia, Synthetic indole and melatonin derivatives exhibit antimalarial activity on the cell cycle of the human malaria parasite Plasmodium falciparum, Eur. J. Med. Chem. 78 (2014) 375–382, https://doi.org/10.1016/j.ejmech.2014.03.055.

[27] M.C. Joshi, K.J. Wicht, D. Taylor, R. Hunter, P.J. Smith, T.J. Egan, In vitro antimalarial activity, β-haematin inhibition and structure-activity relationships in a series of quinoline triazoles, Eur. J. Med. Chem. 69 (2013), https://doi.org/10.1016/j.ejmech.2013.08.046.

[28] J.N. Okoyeh, C.R. Pillai, C.E. Chitnis, Plasmodium falciparum field isolates commonly use erythrocyte invasion pathways that are independent of sialic acid residues of glycophorin A, Infect. Immun. 67 (1999) 5784–5791, https://doi.org/10.1128/iai.67.11.5784-5791.1999.

[29] I. Wadi, C.R. Pillai, A.R. Anvikar, A. Sinha, M. Nath, N. Valecha, Methylene blue induced morphological deformations in Plasmodium falciparum gametocytes: implications for transmission-blocking, Malar. J. 17 (2018) 11, https://doi.org/10.1186/s12936-017-2153-9.

[30] I. Wadi, N. Deora, M. Nath, A. Sinha, Investigation of factors affecting the production of P. falciparum gametocytes in an Indian isolate, 3 Biotech 11 (2021) 55, https://doi.org/10.1007/s13205-020-02586-7.

[31] H.A. Antony, V. Pathak, K. Ghosh, S.C. Parija, Comparison of protein expression pattern between the Plasmodium falciparum chloroquine-resistant RKL9 and chloroquine-sensitive MRC2 strains, Trop. Parasitol. 6 (2016) 136–140, https://doi.org/10.4103/2229-5070.190831.

[32] B. Aneja, R. Arif, A. Perwez, J.V. Napoleon, P. Hasan, M.M.A. Rizvi, A. Azam, Rahisuddin, M. Abid, N-substituted 1,2,3-Triazolyl-appended indole-chalcone hybrids as potential DNA Intercalators endowed with antioxidant and anticancer properties, ChemistrySelect 3 (2018) 2638–2645, https://doi.org/10.1002/slct.201702913.

[33] K. Xue, G. Sun, Y. Zhang, X. Chen, Y. Zhou, J. Hou, H. Long, Z. Zhang, M. Lei, W. Wu, A new method for the synthesis of chalcone derivatives promoted by PPh3/I2 under non-alkaline conditions, Synth. Commun. 51 (2021), https://doi.org/10.1080/00397911.2020.1847295.

[34] V. Rajkumar, S.A. Babu, R. Padmavathi, Regio- and diastereoselective construction of a new set of functionalized pyrrolidine, spiropyrrolidine and spiropyrrolizidine scaffolds appended with aryl- and heteroaryl moieties via the azomethine ylide cycloadditions, Tetrahedron 72 (2016), https://doi.org/10.1016/j.tet.2016.07.053.

[35] S.A. Gamage, J.A. Spicer, G.J. Atwell, G.J. Finlay, B.C. Baguley, W.A. Denny, Structure-activity relationships for substituted bis(acridine-4- carboxamides): a new class of anticancer agents, J. Med. Chem. 42 (1999), https://doi.org/10.1021/jm980687m.

[36] A. Uddin, V. Singh, I. Irfan, T. Mohammad, R.S. Hada, M.I. Hassan, M. Abid, S. Singh, Identification and structure–activity relationship (SAR) studies of carvacrol derivatives as potential anti-malarial against Plasmodium falciparum falcipain-2 protease, Bioorg. Chem. 103 (2020), https://doi.org/10.1016/j.bioorg.2020.104142.

[37] M. Irfan, B. Aneja, U. Yadava, S.I. Khan, N. Manzoor, C.G. Daniliuc, M. Abid, Synthesis, QSAR and anticandidal evaluation of 1,2,3-triazoles derived from naturally bioactive scaffolds, Eur. J. Med. Chem. 93 (2015) 246–254, https://doi.org/10.1016/j.ejmech.2015.02.007.

[38] B. Aneja, M. Azam, S. Alam, A. Perwez, R. Maguire, U. Yadava, K. Kavanagh, C.G. Daniliuc, M.M.A. Rizvi, Q.M.R. Haq, M. Abid, Natural product-based 1,2,3-triazole/sulfonate analogues as potential chemotherapeutic agents for bacterial infections, ACS Omega 3 (2018) 6912–6930, https://doi.org/10.1021/acsomega.8b00582.

[39] H.B. Reilly, H. Wang, J.A. Steuter, A.M. Marx, M.T. Ferdig, Quantitative dissection of clone-specific growth rates in cultured malaria parasites, Int. J. Parasitol. 37 (2007), https://doi.org/10.1016/j.ijpara.2007.05.003.

[40] M.T. Makler, J.M. Ries, J.A. Williams, J.E. Bancroft, R.C. Piper, B.L. Gibbins, D.J. Hinrichs, Parasite lactate dehydrogenase as an assay for Plasmodium falciparum drug sensitivity, Am. J. Trop. Med. Hyg. 48 (1993) 739–741, https://doi.org/10.4269/ajtmh.1993.48.739.

[41] V. Singh, R.S. Hada, R. Uddin, B. Aneja, M. Abid, K.C. Pandey, S. Singh, Inhibition of hemoglobin degrading protease falcipain-2 as a mechanism for anti-malarial activity of triazole-amino acid hybrids, Curr. Top. Med. Chem. 20 (2020) 377–389, https://doi.org/10.2174/1568026620666200130162347.

[42] T.T. Men, N.T. Huy, D.T.X. Trang, M.N. Shuaibu, K. Hirayama, K. Kamei, A simple and inexpensive haemozoin-based colorimetric method to evaluate anti-malarial drug activity, Malar. J. 11 (2012), https://doi.org/10.1186/1475-2875-11-272.

[43] B.C. Evans, C.E. Nelson, S.S. Yu, K.R. Beavers, A.J. Kim, H. Li, H.M. Nelson, T.D. Giorgio, C.L. Duvall, Ex vivo red blood cell hemolysis assay for the evaluation of pH-responsive endosomolytic agents for cytosolic delivery of biomacromolecular drugs, J. Vis. Exp. (2013), https://doi.org/10.3791/50166.

[44] H.J. Woerdenbag, T.A. Moskal, N. Pras, T.M. Malingré, F.S. El-Feraly, H.H. Kampinga, A.W.T. Konings, Cytotoxicity of artemisinin-related endoperoxides to Ehrlich ascites tumor cells, J. Nat. Prod. 56 (1993) 849–856, https://doi.org/10.1021/np50096a007.

[45] F.A. Wani, Amaduddin, B. Aneja, G. Sheehan, K. Kavanagh, R. Ahmad, M. Abid, R. Patel, Synthesis of novel benzimidazolium gemini surfactants and evaluation of their anti-Candida activity, ACS Omega 4 (2019), https://doi.org/10.1021/acsomega.9b01056.

[46] A. Daina, O. Michielin, V. Zoete, SwissADME: a free web tool to evaluate pharmacokinetics, drug-likeness and medicinal chemistry friendliness of small molecules, Sci. Rep. 7 (2017), https://doi.org/10.1038/srep42717.

[47] L. Zhang, H. Ai, W. Chen, Z. Yin, H. Hu, J. Zhu, J. Zhao, Q. Zhao, H. Liu, CarcinoPred-EL, Novel models for predicting the carcinogenicity of chemicals using molecular fingerprints and ensemble learning methods, Sci. Rep. 7 (2017), https://doi.org/10.1038/s41598-017-02365-0.

[48] S. Duhr, D. Braun, Why molecules move along a temperature gradient, Proc. Natl. Acad. Sci. U. S. A. 103 (2006), https://doi.org/10.1073/pnas.0603873103.

[49] C.J. Wienken, P. Baaske, U. Rothbauer, D. Braun, S. Duhr, Protein-binding assays in biological liquids using microscale thermophoresis, Nat. Commun. 1 (2010) 100, https://doi.org/10.1038/ncomms1093.

[50] R. Jain, S. Gupta, M. Munde, S. Pati, S. Singh, Development of novel anti-malarial from structurally diverse library of molecules, targeting plant-like CDPK1, a multistage growth regulator of P. falciparum, Biochem. J. 447 (2020), https://doi.org/10.1042/BCJ20200045.

[51] R. Jain, P. Dey, S. Gupta, S. Pati, A. Bhattacherjee, M. Munde, S. Singh, Molecular dynamics simulations and biochemical characterization of Pf14-3-3 and PfCDPK1 interaction towards its role in growth of human malaria parasite, Biochem. J. 477 (2020), https://doi.org/10.1042/BCJ20200145.

[52] D. Ramu, R. Jain, R.R. Kumar, V. Sharma, S. Garg, R. Ayana, T. Luthra, P. Yadav, S. Sen, S. Singh, Design and synthesis of imidazolidinone derivatives as potent anti-leishmanial agents by bioisosterism, Arch. Pharm. (Weinheim) (2019) 352, https://doi.org/10.1002/ardp.201800290.

[53] M.V.N. de Souza, K.C. Pais, C.R. Kaiser, M.A. Peralta, M. de L. Ferreira, M.C.S. Lourenço, Synthesis and in vitro antitubercular activity of a series of quinoline derivatives, Bioorganic Med. Chem. 17 (2009), https://doi.org/10.1016/j.bmc.2009.01.013.

[54] B. Aneja, A. Queen, P. Khan, F. Shamsi, A. Hussain, P. Hasan, M.M.A. Rizvi, C.G. Daniliuc, M.F. Alajmi, M. Mohsin, M.I. Hassan, M. Abid, Design, synthesis & biological evaluation of ferulic acid-based small molecule inhibitors against tumor-associated carbonic anhydrase IX, Bioorganic Med. Chem. 28 (2020) 115424, https://doi.org/10.1016/j.bmc.2020.115424.

[55] J.A. Rowe, A. Claessens, R.A. Corrigan, M. Arman, Adhesion of Plasmodium falciparum-infected erythrocytes to human cells: molecular mechanisms and therapeutic implications, Expert Rev. Mol. Med. 11 (2009) 1–29, https://doi.org/10.1017/S1462399409001082.

[56] N.T. Huy, Y. Shima, A. Maeda, T.T. Men, K. Hirayama, A. Hirase, A. Miyazawa, K. Kamei, Phospholipid membrane-mediated hemozoin formation: the effects of physical properties and evidence of membrane surrounding hemozoin, PLoS One 8 (2013), https://doi.org/10.1371/journal.pone.0070025.

[57] A.P. Gorka, J.N. Alumasa, K.S. Sherlach, L.M. Jacobs, K.B. Nickley, J.P. Brower, A.C. De Dios, P.D. Roepe, Cytostatic versus cytocidal activities of chloroquine analogues and inhibition of hemozoin crystal growth, Antimicrob. Agents Chemother. 57 (2013) 356–364, https://doi.org/10.1128/AAC.01709-12.

[58] N.T. Huy, K. Kamei, T. Yamamoto, Y. Kondo, K. Kanaori, R. Takano, K. Tajima, S. Hara, Clotrimazole binds to heme and enhances heme-dependent hemolysis: proposed antimalarial mechanism of clotrimazole, J. Biol. Chem. 277 (2002) 4152–4158, https://doi.org/10.1074/jbc.M107285200.

[59] S.E. Francis, D.J. Sullivan, D.E. Goldberg, Hemoglobin metabolism in the malaria parasite Plasmodium falciparium, Annu. Rev. Microbiol. 51 (1997) 97–123, https://doi.org/10.1146/annurev.micro.51.1.97.

[60] B. Tekwani, L. Walker, Targeting the hemozoin synthesis pathway for new antimalarial drug discovery: Technologies for in vitro β-hematin formation assay, Comb. Chem. High Throughput Screen. 8 (2005) 63–79, https://doi.org/10.2174/1386207053328101.

[61] N. Kato, T. Sakata, G. Breton, K.G. Le Roch, A. Nagle, C. Andersen, B. Bursulaya, K. Henson, J. Johnson, K.A. Kumar, F. Marr, D. Mason, C. McNamara, D. Plouffe, V. Ramachandran, M. Spooner, T. Tuntland, Y. Zhou, E.C. Peters, A. Chatterjee, P.G. Schultz, G.E. Ward, N. Gray, J. Harper, E.A. Winzeler, Gene expression signatures and small-molecule compounds link a protein kinase to Plasmodium falciparum motility, Nat. Chem. Biol. 4 (2008) 347–356, https://doi.org/10.1038/nchembio.87.

[62] G. Lemercier, A. Fernandez-Montalvan, J.P. Shaw, D. Kugelstadt, J. Bomke, M. Domostoj, M.K. Schwarz, A. Scheer, B. Kappes, D. Leroy, Identification and characterization of novel small molecules as potent inhibitors of the plasmodial calcium-dependent protein kinase 1, Biochemistry 48 (2009) 6379–6389, https://doi.org/10.1021/bi9005122.

[63] J. Baell, M.A. Walters, Chemistry: chemical con artists foil drug discovery, Nature 513 (2014) 481–483, https://doi.org/10.1038/513481a.

[64] S.E.A. Ozbabacan, H.B. Engin, A. Gursoy, O. Keskin, Transient protein–protein interactions, Protein Eng. Des. Sel. 24 (2011), https://doi.org/10.1093/protein/gzr025.

[65] C.H. Kaschula, T.J. Egan, R. Hunter, N. Basilico, S. Parapini, D. Taramelli, E. Pasini, D. Monti, Structure - activity relationships in 4-aminoquinoline antiplasmodials. The role of the group at the 7-position, J. Med. Chem. 45 (2002), https://doi.org/10.1021/jm020858u.

[66] F. Xu, Z.Z. Yang, J.R. Jiang, W.G. Pan, X. Le Yang, J.Y. Wu, Y. Zhu, J. Wang, Q.Y. Shou, H.G. Wu, Synthesis, antitumor evaluation and molecular docking studies of [1,2,4]triazolo[4,3-b][1,2,4,5]tetrazine derivatives, Bioorganic Med. Chem. Lett. 26 (2016), https://doi.org/10.1016/j.bmcl.2016.05.007.

[67] H.A.M. El-Sherief, B.G.M. Youssif, S.N.A. Bukhari, M. Abdel-Aziz, H.M. Abdel-Rahman, Novel 1,2,4-triazole derivatives as potential anticancer agents: design, synthesis, molecular docking and mechanistic studies, Bioorg. Chem. 76 (2018), https://doi.org/10.1016/j.bioorg.2017.12.013.

[68] H.A.M. Goma'a, M.A. Ghaly, L.A. Abou-zeid, F.A. Badria, I.A. Shehata, M.M. El-Kerdawy, Synthesis, biological evaluation and in silico studies of 1,2,4-triazole and 1,3,4-thiadiazole derivatives as antiherpetic agents, ChemistrySelect 4 (2019), https://doi.org/10.1002/slct.201900814.